12CO(J = 1 \to 0) On-the-fly Mapping Survey of the Virgo Cluster Spirals. II. Molecular Gas Properties in Different Density Environments

Chung, Eun Jung; Yun, Min S.; Verheijen, Marc A. W.; Chung, Aeree

Published in:
The Astrophysical Journal

DOI:
10.3847/1538-4357/aa756b

The Astrophysical Journal, 843:50 (21pp), 2017 July 1 https://doi.org/10.3847/1538-4357/aa756b

^{12}CO($J = 1 \rightarrow 0$) On-the-fly Mapping Survey of the Virgo Cluster Spirals. II. Molecular Gas Properties in Different Density Environments

Eun Jung Chung[1], Min S. Yun[2], Marc A. W. Verheijen[3], and Aeree Chung[4]
[1] Korea Astronomy and Space Science Institute, 776 Daedeokdae-ro, Yuseong-gu, Daejeon 34055, Korea; ejchung@kasi.re.kr
[2] Department of Astronomy, University of Massachusetts, Amherst, MA 01003, USA
[3] Kapteyn Astronomical Institute, University of Groningen, Postbus 800, 9700 AV Groningen, The Netherlands
[4] Department of Astronomy, Yonsei University, 50 Yonsei-ro, Seodaemun-gu, Seoul 03722, Korea
Received 2016 October 2; revised 2017 May 23; accepted 2017 May 25; published 2017 June 30

Abstract

This study investigated the properties of the molecular gas content and star formation activity of 17 Virgo spirals, 21 Ursa Major (UMa) spirals, 13 Pisces spiral galaxies, and a comparison sample of 11 field spiral galaxies with a spatially resolved gas and stellar distribution. The H I-deficient galaxies with a $\mathrm{def}_{\mathrm{H\,I}} > 0.4$ have a similar range of CO luminosity normalized by the *K*-band luminosity ($L_{\mathrm{CO}}/L_{\mathrm{K}}$) like the field spirals, although their CO content can be smaller by up to a factor of 2. The CO, H I, and stellar disk diameters are closely related to each other for both cluster and field galaxies, and the relative diameters of the CO and H I disks grow monotonically and smoothly as the H I-to-stellar disk diameter ratio decreases. Cluster galaxies have a molecular gas consumption time up to 10 times shorter than that of the field comparison sample, suggesting a significant change in the molecular gas content and star formation activity among all the cluster galaxies, even when they do not show any sign of H I stripping. The strongly H I-stripped Virgo cluster galaxies show only a modestly reduced total gas consumption time, indicating that the star formation activity and gas consumption are a highly local (rather than global) phenomenon. Our finding is that the depletion of cold gas by ram-pressure stripping and/or starvation caused by preprocessing in each cluster environment makes galaxies evolve passively.

Key words: galaxies: clusters: individual (Virgo, Ursa Major, Pisces) – galaxies: evolution – galaxies: star formation – ISM: molecules

1. Introduction

Atomic hydrogen gas is known as a reservoir for future star formation in a galaxy and is supposed to be the transitionary phase in the accretion processes between the warm halo/intergalactic medium (IGM) and the cold molecular hydrogen gas. The extraplanar H I gas, warped outer layers, and H I complexes of tails and filament shapes are ubiquitous (e.g., Bosma 1991; Putman et al. 2012). Besides, the rate of star formation in the Milky Way, especially in the solar vicinity, has been rather constant during the last 10 Gyr (e.g., Binney et al. 2000; Fraternali & Tomassetti 2012), and the cosmic SFR density has dropped by a factor of 10 since $z = 2$ (e.g., Hopkins & Beacom 2006), while $\mathrm{Omega}_{\mathrm{H\,I}}$ has been formally constant from $z = 5$ to $z \sim 0.5$ (see Figure 12 of Crighton et al. 2015). All these point out the need for gas replenishment to sustain the star formation rate in the late type of galaxies (Sancisi et al. 2008; Sánchez Almeida et al. 2014).

There are several accretion mode channels that may be interrupted by various physical processes that depend both on the galaxy mass and the environment. The mode of accretion, i.e., hot accretion, cold accretion, or mergers, does not only depend on the halo mass but also on the environment (e.g., Dekel & Birnboim 2006; Fumagalli et al. 2016; Geréb et al. 2016), and the same is true for gas removal like ram-pressure stripping and depletion processes such as consumption due to SF (e.g., Gunn & Gott 1972; Bekki et al. 2002). Furthermore, in massive disk galaxies, one would expect hot accretion as the inflowing gas gets shock-heated to the virial temperature but the postulated Galactic Fountain in a star-forming disk could cool this hot halo gas in the disk−halo interface and bring it down into the disk where it becomes available for star formation through the molecular phase (see Fu et al. 2010; Kauffmann et al. 2012).

Understanding which channel of accretion mode and interruption is efficient in which environment is important because it reveals how a galaxy forms and evolves. Galactic properties widely vary with morphology (e.g., Roberts & Haynes 1994; Young et al. 1996). Early-type galaxies are red in color with smoothly varying brightness, old stars, and generally no gas (no star formation). Meanwhile, late-type galaxies are blue in color with spiral arms where young stars and cool gas are present. The discrepancy in the color and composition of the stars and gas between the early- and late-type galaxies shows that these galaxies have different star formation histories. The overall environment is also found to change with the morphology in a way that the fraction of spiral galaxies decreases from 80% in the field to 60% in the outskirts of clusters to close to zero in the cores of rich clusters (Dressler 1980; Whitmore et al. 1993).

As a result, the gas and star formation properties of galaxies in a high-density region such as the core of galaxy clusters have been observed to be different from those in the field. Cluster galaxies are redder (Kennicutt 1983) and have less atomic hydrogen gas (Chamaraux et al. 1980; Giovanelli & Haynes 1983; Serra et al. 2012). In fact, much evidence for interstellar gas removal in the cluster environment such as ram-pressure stripping or thermal evaporation has already been found in many H I imaging studies (e.g., Cayatte et al. 1990, 1994; Bravo-Alfaro et al. 2000; Chung et al. 2009a). In addition, the star formation activity of spiral galaxies in clusters is found to be low compared to that of field spirals (e.g., Balogh et al. 1998; Gavazzi et al. 2002b; Koopmann & Kenney 2004a, 2004b; Jaffé et al. 2016; Penny et al. 2016), which

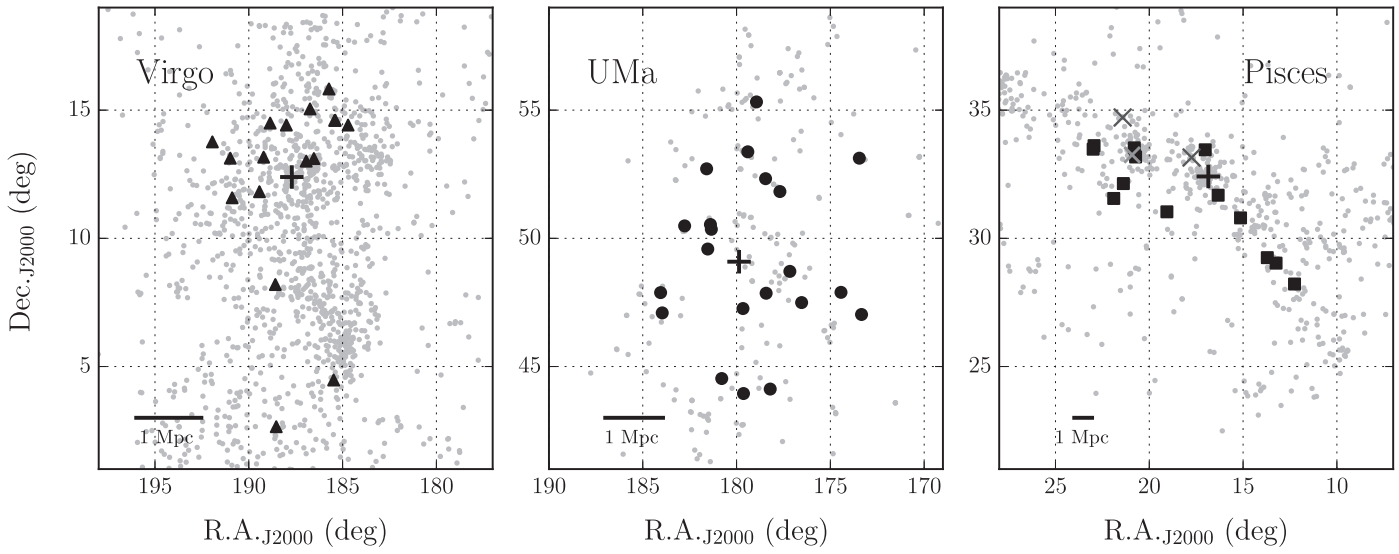

Figure 1. Projection on the sky of all galaxies of the Virgo (left), UMa (middle), and Pisces (right) clusters with gray dots. The cluster center denoted with the plus symbol is the position of M87, a giant elliptical galaxy, for Virgo (R.A. = $11^{h}59^{m}28\overset{s}{.}3$, decl. = $49^{d}5^{m}17\overset{s}{.}8$ in J2000) and for UMa following Tully et al. (1996), and the position of NGC 383, which is a bright radio galaxy (3C 31; see Hardcastle et al. 2002 and references therein) for the Pisces cluster. The small crosses in the rightmost panel indicate the central positions of the N410, N507, and N529 galaxy groups (Sakai et al. 1994). Virgo galaxies are from the Extended Virgo Cluster Catalog (Kim et al. 2014), UMa galaxies are from NED (NASA/IPAC Extragalactic Database, http://ned.ipac.caltech.edu) within 10° radius from the given cluster center and velocity range of 700 and 1210 km s^{-1} (Tully et al. 1996), and Pisces galaxies are from NED within 10° radius from NGC 383 and the velocity range of 4000–6000 km s^{-1} (Giovanelli & Haynes 1985; Sakai et al. 1994), respectively. The horizontal bar at the lower left corner represents the 1 Mpc physical scale assuming distances of 16.5 Mpc, 18.6 Mpc, and 60.3 Mpc for the Virgo, UMa, and Pisces clusters, and the sample galaxies of the Virgo, UMa, and Pisces cluster in this paper are denoted with filled triangles, circles, and squares, respectively.

Table 1
Properties of the Virgo, UMa, and Pisces Clusters of Galaxies

	Location		Distance	Virial Radius	Number of Member Galaxies	Velocity Dispersion
	R.A. (J2000)	Decl. (J2000)	(Mpc)	(Mpc)		(km s^{-1})
Virgo	$12^{h}30^{m}49\overset{s}{.}4$	12° 23′ 28″	16.5 (1)	∼0.73 (2)	∼1600 (3)	∼715 (2)
UMa	$11^{h}59^{m}28\overset{s}{.}3$	49° 5′ 17″.8	18.6 (4)	∼0.88 (2)	166 (5)	∼148 (2)
Pisces	$1^{h}7^{m}24\overset{s}{.}9$	32° 24′ 45″	60.3 (4)	∼1.3 (6)	63 (6)	···

Note. The location of the Virgo cluster is assigned with M87, a giant elliptical galaxy, and that of the UMa cluster is from Tully et al. (1996). For the Pisces cluster, the position of NGC 383, a bright radio galaxy, is provided.
References. (1) Mei et al. (2007), (2) Tully et al. (1996), (3) Kim et al. (2014), (4) Tully & Pierce (2000), (5) Pak et al. (2014), (6) Hanski et al. (2001).

could well be relevant to interstellar gas stripping. Indeed, the formation and evolution of a galaxy is a collaboration of the ISM, the building materials, and the environment where a galaxy settles down.

It has been well established that molecular clouds are sites of ongoing star formation (Larson 2003 and references therein), and any effect of the environment on the molecular gas in a galaxy can have an effect on the star formation activity and thus on the evolution of spiral galaxies. Previous studies on the molecular gas contents, however, have reached varying and sometimes opposite conclusions. By comparing Virgo and/or Coma spiral galaxies with field counterparts, Stark et al. (1986), Kenney & Young (1989), Casoli et al. (1991), Boselli et al. (1997), and Perea et al. (1997) found that the CO luminosity of the spirals was comparable in the cluster and field environments. This suggests that galaxies may not lose their molecular gas easily like atomic gas. This is understandable because molecular gas usually resides in the inner disk, i.e., in a deeper gravitational potential well, whereas Rengarajan & Iyengar (1992) reported some molecular gas deficiency for almost the same sample as that of Kenney & Young (1989). In addition, more recent studies such as those by, Fumagalli et al. (2009), Scott et al. (2013) and Boselli et al. (2014a, 2014b, 2014c) found that the molecular gas density is lower in severely H I-stripped galaxies claiming that the environment essentially affects the molecular gas.

The fact that the molecular gas is deficiency is not as clear as that of the atomic gas and is therefore still debatable is indeed puzzling. This is because a molecular cloud is known to be the site of ongoing star formation, yet cluster galaxies are obviously less active in forming stars compared to their field counterparts. Therefore, this work revisited the molecular gas deficiency of galaxies located in a range of density environments. Specifically, by increasing the number of samples in low density environments, the mean molecular gas fraction of late-type galaxies was recalibrated. Moreover, by comparing

the global and spatially resolved H I and CO properties of similar galaxies in different cosmic environments, a better understanding was obtained of the connecting link between the accretion gas and star formation as well as insights into which process is relevant in which environments.

This study investigated and compared the CO properties of Virgo cluster spiral galaxies with those of Ursa Major (hereafter UMa) and Pisces spiral galaxies. The spatial distribution of the galaxies are presented in Figure 1, and the characteristics of the clusters are listed in Table 1.

The Virgo cluster is one of the best samples when studying environmental effects because its dynamical evolution is still in progress, where hot intracluster gas extends over most of the optically visible cluster (Böhringer et al. 1994) and evidence of significant environmental effects is ubiquitous (e.g., Chung et al. 2007; Kenney et al. 2014).

For these reasons, the Virgo cluster has been observed at various wavelengths. It is the first cluster for which significant H I imaging was done (van Gorkom et al. 1984), and various H I surveys, such as by Warmels (1986), Cayatte et al. (1990), and recently the ALFALFA (Giovanelli et al. 2007) and VIVA (Chung et al. 2009a) surveys, have been conducted. Many recent multiwavelength data are also available for the Virgo cluster galaxies, such as the radio continuum by the NRAO VLA Sky Survey (NVSS; Condon et al. 1998), the Hα by Koopmann et al. (2001) and Gavazzi et al. (2002a), the UV survey by FAUST (Brosch et al. 1997) and *GALEX* (Boselli et al. 2011; Voyer et al. 2014), and the IR surveys by *Spitzer* (Kenney et al. 2012). High-quality optical images are also available from the *HST*/ACS Virgo Cluster Survey (Côté et al. 2004), and many studies have been done with the Sloan Digital Sky Survey (SDSS; e.g., Lisker et al. 2006a, 2006b, 2007, 2008; Chen et al. 2010; Kim et al. 2014).

The environmental effects and mechanisms, especially the ram-pressure effect, have been investigated in detail for the Virgo cluster galaxies. For example, ICM−ISM stripping and the tidal interaction from H I observations and simulations (e.g., Vollmer et al. 2001, 2004; Chung et al. 2007) and quenching have been investigated as well as the enhancement of star formation by ram pressure and the fate of galaxies (e.g., Koopmann & Kenney 2004a, 2004b; Crowl & Kenney 2008; Kenney et al. 2014; Boselli et al. 2016a, 2016b).

The UMa cluster is located at roughly the same distance as the Virgo cluster. However, its environment is significantly different from that of the Virgo cluster. While the Virgo cluster has a giant elliptical galaxy, M87, at the cluster center, UMa does not have any concentration toward any center. Its galaxy density is one order of magnitude lower than that of the Virgo cluster, and the dominant population of the UMa cluster is late-type spirals. No X-ray emissions have been detected; thus, most UMa spiral galaxies are normal in H I content (Verheijen 1995, 2004; Verheijen & Sancisi 2001). Its velocity dispersion is relatively small at $\sim$148 km s^{-1} compared with $\sim$715 km s^{-1} for the Virgo cluster (Tully et al. 1996), and it has been inferred that the UMa cluster is in an early stage of collapse (Wolfinger et al. 2016).

The UMa cluster provides a unique laboratory to study the effect of tidal interaction between galaxies as well as the effect of preprocessing in the group environment. Verheijen (2001) reported the global H I morphologies for the UMa spiral galaxies, and 25% of the 56 spirals show a warp in the H I disk; 25% have a morphological lopsidedness (kinematical lopsidedness is also found in one-fourth of the spirals), and 16% have a tidal H I tail. Wolfinger et al. (2013) did a H I blind survey of the UMa region and found that 33% of the H I sources have multiple optical counterparts indicating a tidal interaction. Recently, Wolfinger et al. (2016) redefined the UMa cluster as a supergroup consisting of six groups and found that UMa galaxies included in galaxy groups tend to be deficient in H I, and they are merging and forming a poor cluster, eventually infalling into the Virgo cluster.

The Pisces cluster (also called the Pisces filament) is one of the major groups of galaxies in the Perseus−Pisces supercluster, the most prominent large-scale structure in the local universe, which covers $\sim$50° across the northern sky and contains $\sim$200 groups of galaxies (e.g., Haynes & Giovanelli 1986; Hanski et al. 2001). The Perseus−Pisces supercluster has a filamentary structure whose depth is approximately the same as its extent on the sky and is perhaps still in an early evolutionary stage accreting neighboring smaller groups and galaxies (Sakai et al. 1994; Sakai 1995). The NGC 383 and NGC 507 galaxy groups, which are the densest regions in the Pisces cluster (e.g., Arp 1968; Sakai et al. 1994), have been detected by X-ray, and the X-ray emission extends to $\sim$1 Mpc and 500 kpc from NGC 383 and NGC 507, respectively (Kim & Fabbiano 1995; Komossa & Böhringer 1999; Kraft et al. 2004). Because of the early evolutionary stage of the Pisces cluster and the small range of the X-ray emissions, it is supposed that galaxies that are affected by the ICM pressure are rare, and most of the spiral galaxies in the Pisces cluster are normal in H I content.

The specific questions this study addresses are as follows. (1) Are there any systematic differences in the CO properties of spiral galaxies in various density environments? In particular, are H I-stripped Virgo spirals also deficient in CO? (2) How do different molecular gas properties result in star formation activities and thus galaxy evolution? The remainder of this paper is organized as follows. In Section 2, the sample and data are described. The CO properties in different environments are examined in Section 3. The relation of star formation and gas properties is shown in Section 4. A summary and the conclusion are given in Section 5.

2. Sample and Data

2.1. Spiral Galaxies in the Galaxy Clusters

2.1.1. Sample

This study examined 17 spiral galaxies of the Virgo cluster, 21 spirals of the UMa cluster, and 13 spirals of the Pisces cluster.

The Virgo sample is essentially the same as the sample used by Chung et al. (2009b) initially selected from the study by Kenney & Young (1988). In the CO mapping study of Chung et al. (2009b), 28 Virgo galaxies were initially chosen based on the angular size and the single-dish CO flux, and 20 galaxies have been detected in the imaging study. Among these, this study excluded the galaxy pair of NGC 4567 and 4568, which are hardly separated spatially and kinematically. NGC 4536 was also excluded in this study because it is observed only at the central region. Finally, this study used 17 galaxies in the analysis presented in this paper. The Virgo sample spans a range of morphological types of Sa−Scd with optical diameters

of 3–10 arcmin and a B-band magnitude of $9 \lesssim B_T^0 \lesssim 12$ mag, and the distribution of the galaxies in the cluster is also wide ($1^\circ \lesssim R_{\rm M87} \lesssim 10^\circ$).

For the UMa sample, this study adopted the sample from the CO imaging study by A. Chung et al. (2017, in preparation) selected from Tully et al. (1996). The complete volume-limited optical sample consists of 62 galaxies that meet the following conditions: (1) $700 < V_{\rm sys} < 1210\,{\rm km\,s^{-1}}$, (2) $R < 7^\circ.5$, where R is the projected distance from $11^{\rm h}59^{\rm m}28^{\rm s}.3$ and $49^{\rm d}5^{\rm m}17^{\rm s}.8$ (J2000), and (3) $m_{\rm Zwicky} < 14.5$ mag. Among these, 21 galaxies that are brighter than 10 mag in $m_{\rm K'}$, larger than ~2.75 arcmin in D_{25}, and H I-detected, are observed.

The Pisces cluster sample is a subsample of Giovanelli & Haynes (1985), who did a H I survey of the declination zone $+27^\circ.5$ to $+33^\circ.5$ of the Pisces–Perseus supercluster. The sample galaxies used in this study are located in an R.A. range of $0^{\rm h}49^{\rm m}$ and $01^{\rm h}\ 32^{\rm m}$ along the filament structure of the galaxies, and the heliocentric velocity range is ~4000 and $6000\,{\rm km\,s^{-1}}$. This study constructed a magnitude-limited sample selected from Tully & Pierce (2000) and carried out single-dish observations of 13 galaxies in the order of the FIR flux to increase the detection rate.

2.1.2. CO Data

For the Virgo and UMa samples, on-the-fly (OTF) mapping data were used, which cover the full extents of the stellar disks. Due to the large distance, the spiral galaxies of the Pisces cluster have been observed with a point observation.

The CO data of the Virgo spiral galaxies used here come from the $^{12}{\rm CO}(J = 1 - 0)$ OTF Mapping Survey carried out with the 14 m telescope of the Five College Radio Astronomy Observatory (FCRAO) using the SEQUOIA (SEcond QUabbin Optical Imaging Array; Chung et al. 2009b). The angular resolution at 115 GHz is 45″ (~3.7 kpc at a distance of 16.5 Mpc). The backend system the Quabbin Extragalactic Filterbanks (QEF) was used, which consists of 16 independent spectrometers providing 64 channels at a 5 MHz resolution (velocity resolution of $\sim 13\,{\rm km\,s^{-1}}$ at 115 GHz). The OTF observations have fully covered the entire stellar disk of each galaxy multiple times, and typically, a $10' \times 10'$ size map centered on each galaxy is obtained. Data reduction was carried out in two steps, initially using the revised-OTFTOOL and later the GIPSY (Groningen Image Processing SYstem; van der Hulst et al. 1992)[5] package.

CO maps of the UMa sample galaxies were obtained from the NRAO 12 m telescope at Kitt Peak in the OTF mode from two observational runs during 1999 June 20–27 and 2000 March 23–30. The angular resolution of the antenna is 55″ at 115 GHz (~5.0 kpc at a distance of 18.6 Mpc). Two polarizations were used consisting of 256 channel filter banks, with each channel having a width of 2 MHz (velocity resolution of $5.2\,{\rm km\,s^{-1}}$). The galaxies have been fully observed with a size of at least $7'.5 \times 7'.5$. Data reduction was done with *otfmakeoffs*, a package implemented in AIPS (Astronomical Image Processing System)[6] and further processed with GIPSY (Rhee et al. 2001, A. Chung et al. 2017, in preparation).

The CO spectra of the Pisces spiral galaxies were obtained with the NRAO 12 m telescope at Kitt Peak, which were performed from 1999 June through 2000 March. The optical diameter of the Pisces sample used in this study ranges from 1 to 2 arcmin. Considering that CO extends out to about half the optical disk in most galaxies (Young et al. 1995), each galaxy was observed by a single point with a beam size of ~55″ at 115 GHz, which should be large enough to cover the entire CO disk for the Pisces sample. Dual channel 3 mm receivers were used to observe two polarizations and averaged for better sensitivity. Two filter bank spectrometers consisting of 256 channels with a 2 MHz frequency resolution (velocity resolution of $5.2\,{\rm km\,s^{-1}}$) were used. The data taken in the $T_{\rm R}^*$ scale were corrected by the main-beam efficiency $\eta_{\rm mb}^* = 0.88$ and converted into the main-beam brightness temperature $T_{\rm mb}$ (Lavezzi & Dickey 1998). Data reduction of the spectral lines such as a baseline subtraction and smoothing of the spectra was performed with CLASS (Continuum and Line Analysis Single-dish Software), which is one of the GILDAS (Grenoble Image and Line Data Analysis Software)[7] packages (Lee 2007). The CO data of the Pisces galaxies including the CO spectra are presented in Appendix A.1. This study applied the extrapolation method from the single beam observations to the total fluxes following Boselli et al. (2014a, 2014b, 2014c) and used the corrected CO flux throughout this paper (see Appendix A.3).

The CO data used in this study were obtained by different telescopes; thus, the consistency of the fluxes was checked by comparing with the results of the FCRAO extragalactic CO survey (Young et al. 1995) and the Nobeyama CO mapping survey (Kuno et al. 2007). The FCRAO CO survey observed ~300 nearby galaxies with a wide range in the properties. Galaxies larger than 3′ were covered with more than one point along the major axis, while only one point in the center was observed for the small galaxies. All 17 Virgo galaxies and 10 of the 21 UMa galaxies in the sample of this study are included in the sample of the FCRAO survey. None of the Pisces sample used in this study was included in that study. All galaxies except for one UMa spiral galaxy (NGC 3949) have been observed in multiple positions, and the total flux has been calculated using a best-fitting model distribution. The Nobeyama CO mapping survey imaged 40 nearby spiral galaxies covering most of their optical disk between 1995 and 2005 (e.g., Nakai et al. 1994; Kuno & Nakai 1997; Sorai et al. 2000). Among the Virgo and UMa samples used in this study, 11 and 2 galaxies are included in the sample of the Nobeyama imaging study, respectively. Again, none of our Pisces sample was included in that study.

Figure 2 shows the comparisons of the CO fluxes from this study with those from the FCRAO survey and the Nobeyama imaging study. Overall, the fluxes from the different studies are in agreement within measurement errors. In the comparison with the FCRAO study, however, there are several extreme outliers ($>2\sigma$). Big discrepancies are found generally in highly inclined galaxies with $i > 60^\circ$ (N4419, N4298, N3953, N4569, N4438, and N3877), where measured fluxes based on fewer points can result in bigger errors compared to face-on cases. Among less inclined galaxies, N3938 is the only case showing a large difference in the fluxes. This galaxy was observed at six points and detected at four, one of which was detected with an extremely low S/N (~1.5σ). Including this point in the interpolation could have caused a large error. Meanwhile, the fluxes are generally in better agreement between the mapping data from two studies shown on the right panel of Figure 2.

[5] https://astro.rug.nl/~gipsy/
[6] www.aips.nrao.edu
[7] http://iram.fr/IRAMFR/GILDAS

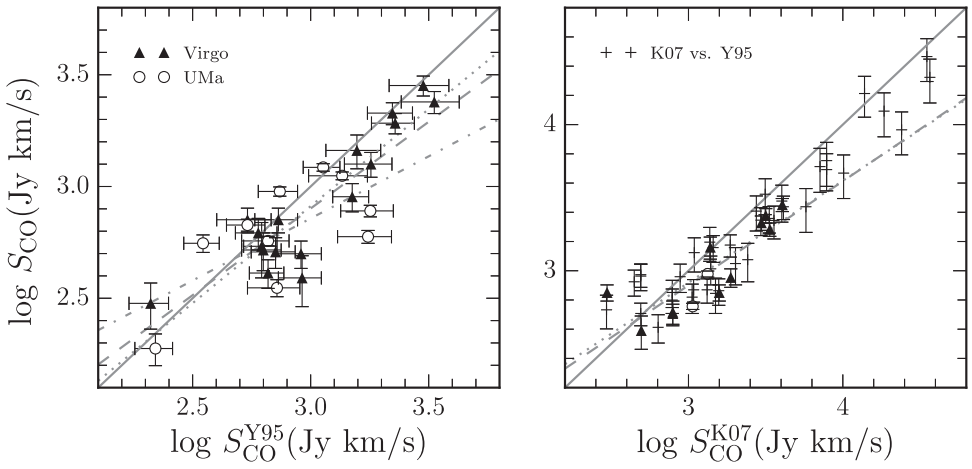

Figure 2. Comparisons of the data used in this paper with those of the FCRAO extragalactic CO survey (Young et al. 1995, left) and the Nobeyama CO mapping survey of nearby spiral galaxies (Kuno et al. 2007, right). Y95 denotes the position-switch measurements reported in the FCRAO extragalactic CO survey data, while K07 refers to the Nobeyama CO mapping survey data. The solid lines indicate the equal flux, and the dotted lines are the least-squares fitting of all data points. The dashed and dashed–dotted lines are the least-squares fitting lines of the Virgo and UMa data, respectively. The gray cross in the right panel shows the comparison of the FCRAO survey data (vertical axis) and the Nobeyama data (horizontal axis).

One extreme outlier, N4548, for which more flux was measured by a factor of >2 (710 versus 300 Jy km s^{-1}), is the case for which the CO flux agrees with that of the FCRAO survey (540 Jy km s^{-1}) within ~1σ uncertainty. This galaxy is almost face-on ($i \sim 37°$), and the sum of the four detected points (not the modeled value) of FCRAO is ~320 Jy km s^{-1} (Kenney & Young 1988). Hence, in this case, the result of the Nobeyama mapping survey could be underestimated.

The CO luminosity is calculated as follows:

$$L_{CO}\,(L_\odot) = 0.119\,d^2\,S_{CO}, \quad (1)$$

where d is the distance to the source in Mpc and S_{CO} is the total CO flux in Jy km s^{-1} (Kenney & Young 1989). The H_2 mass is estimated from the total CO flux measured assuming a linear conversion relation:

$$M_{H2}\,(M_\odot) = 3.9 \times 10^{-17}\,X_{CO}\,d^2\,S_{CO}, \quad (2)$$

where X_{CO} is the CO-to-H_2 conversion factor, d is the distance to the source in megaparsec (Mpc), and S_{CO} is the total CO flux in Jy km s^{-1}. This study used a standard X_{CO} of 2.0×10^{20} mol cm^{-2} (K km s^{-1})$^{-1}$[8] (Bolatto et al. 2013), which does not correct for the contribution of heavy elements, mainly helium. The distances of 16.5, 18.6, and 60.3 Mpc were adopted for the Virgo, UMa, and Pisces spiral galaxies, respectively (Tully & Pierce 2000; Mei et al. 2007).

2.1.3. H I Data

The H I data were taken from Chung et al. (2009a, VIVA survey), Verheijen & Sancisi (2001), and Giovanelli & Haynes (1985) for the Virgo, UMa, and Pisces spiral galaxies, respectively. Among the Virgo sample used in this study, NGC 4303, NGC 4438, NGC 4527, and NGC 4647 are not included in the VIVA survey, and hence, this study used the total H I flux of these galaxies from Cayatte et al. (1990). The H I flux of the Pisces spiral galaxies are from the Arecibo 305 m telescope, and this study does not have the size information for this sample.

The H I mass is determined using the following relation:

$$M_{H\,I}\,(M_\odot) = 2.356 \times 10^5\,d^2\,S_{H\,I}, \quad (3)$$

where d is the distance to the source in Mpc and $S_{H\,I}$ is the total H I flux in Jy km s^{-1}. As a measure of how rich or poor individual galaxies are in atomic gas, the H I deficiency was adopted, which is an empirically designed parameter from the relation of the H I mass with the optical diameter and morphological type of the field spiral galaxies by Haynes & Giovanelli (1984). It is defined as follows:

$$\mathrm{def}_{H\,I} = \langle \log \bar{\Sigma}_{H\,I} \rangle - \log \bar{\Sigma}_{H\,I}, \quad (4)$$

where $\bar{\Sigma}_{H\,I} \equiv S_{H\,I}/D_{opt}^2$, D_{opt} is the optical diameter, and $\langle \log \bar{\Sigma}_{H\,I} \rangle$ is the mean of the field population. This study took the optical diameters from LEDA,[9] which is defined at the 25th magnitude per square arcsec in the B-band. $\langle \log \bar{\Sigma}_{H\,I} \rangle$ is ~0.37 when the morphological type is ignored (Haynes & Giovanelli 1984). Considering this, a $\mathrm{def}_{H\,I}$ of 0.4 is used as the borderline of galaxies with a normal H I content in this work, i.e., H I deficient when $\mathrm{def}_{H\,I} > 0.4$.

2.1.4. Far-ultraviolet (FUV) and Far-infrared (FIR) Data

This study used FUV and FIR data to derive the total bolometric star formation rates of the sample galaxies. UV luminosity is a commonly used SFR indicator under the assumption that the SFR is constant over ~10 to 100 Myr, which is long compared to the lifetime of the dominant UV-emitting population, i.e., stars of ~5 $M_\odot$ or even more massive

[8] X_{CO} can vary with the metallicity and consequently along the Hubble sequence. The sample galaxies used in this study have H-band luminosity-dependent X_{CO} suggested by Boselli et al. (2002) in the range 1–2 × 10^{20} mol cm^{-2} (K km s^{-1})$^{-1}$, and the use of a constant X_{CO} causes a slightly larger scatter in the relationships of H_2 mass and morphological type, optical size, and magnitude than the use of the H-band luminosity-dependent X_{CO}. However, it does not change the results in this work, and hence we choose a constant X_{CO} for consistency between the H_2 mass and CO luminosity.

[9] Lyon/Meudon Extragalactic Database, http://leda.univ-lyon1.fr.

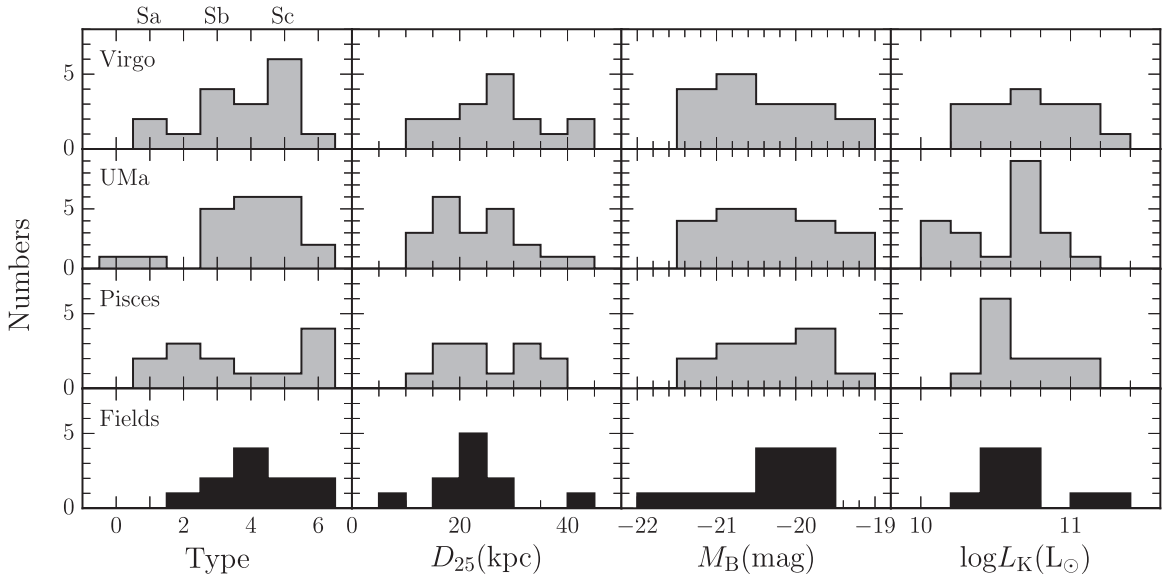

Figure 3. Sample properties as a function of the morphological type (leftmost), the major axis diameter at 25th mag arcsec^{-2} in the *B*-band (second on the left), the absolute *B*-band magnitude corrected for the galactic extinction, internal extinction, and *K*-correction (third on the left), and the total *K*-band luminosity (rightmost).

(Kennicutt 1998). Meanwhile, the FIR continuum at 10–1000 μm mostly originates from dust that absorbs the stellar light and re-emits it. The FIR flux is particularly sensitive to the presence of young and massive stars and can be used as a direct tracer of the star formation activity of galaxies (Devereux & Young 1990). This study used the total bolometric star formation rate, which is defined as the sum of the SFR calculated from the FUV emission (as a tracer of unobscured star formation) and the SFR derived from the FIR emission (as a tracer of obscured star formation; e.g., Murphy et al. 2011; Cybulski et al. 2014).

The FUV flux from the *Galaxy Evolution Explorer* Nearby Galaxy Survey and All-Sky Survey (GR 6) is taken from Lee et al. (2017, in preparation) and Pak et al. (2014) for the Virgo and UMa spirals, respectively. For the Pisces spiral galaxies, photometry was performed with the same method used for Virgo and UMa (for more details, see Pak et al. 2014). In our sample, there are galaxies that are not observed and/or located in the boundary of the observing region, and finally, the FUV fluxes for 14 of the 17 Virgo, 16 of the 21 UMa, and 9 of the 13 Pisces spiral galaxies are obtained.

The FIR flux densities of 60 and 100 μm are taken from Sanders et al. (2003). These are the results of the *Infrared Astronomical Satellite* (*IRAS*; Neugebauer et al. 1984), and the FIR flux in Jy is calculated as

$$f_{\rm FIR} = 1.26 \times (f_{60\mu{\rm m}} \times 2.58 + f_{100\mu{\rm m}})\,({\rm Jy}) \quad (5)$$

following Helou et al. (1988).

From the FUV and FIR data, the total bolometric star formation rate was calculated in this study following Murphy et al. (2011) as follows:

$${\rm SFR_{tot}}(M_\odot\ {\rm yr}^{-1}) = 4.42 \times 10^{-44}(L_{\rm FUV} + 0.88L_{\rm FIR}), \quad (6)$$

where $L_{\rm FUV}$ and $L_{\rm FIR}$ are the FUV and FIR luminosities in erg s^{-1}.

2.2. Field Spiral Galaxies

As a comparison sample to the galaxies in the cluster environment, this study took 11 field spiral galaxies[10] from The H I Nearby Galaxy Survey (THINGS; Walter et al. 2008) and the HERA CO-Line Extragalactic Survey (HERACLES; Leroy et al. 2009). These field sample galaxies are truly isolated except for only one, NGC 3351, which is located in the loose galaxy group of M96. However, the stellar and H I morphologies of NGC 3351 are found to be completely undisturbed (e.g., Walter et al. 2008; Watkins et al. 2014), and hence, the field spirals can be a good comparison sample for the cluster galaxies. They are located at a distance of <15 Mpc and have morphological types of Sab–Scd with optical diameters of ~10–30 kpc, a *B*-band magnitude of ~−22 and −19 mag, and *K*-band[11] luminosities of about 10–11.5 solar luminosity in log.

This study used the H I flux from THINGS to derive the atomic hydrogen gas mass and deficiency. In the case of the CO flux, this study took the data from the HERACLES and derived the CO luminosity and molecular hydrogen gas mass with the standard conversion factor of $X_{\rm CO} = 2.0 \times 10^{20}\,{\rm mol\,cm^{-2}\,(K\,km\,s^{-1})^{-1}}$. The FUV and FIR data from *GALEX* and *IRAS* 60 and 100 μm were used to derive the total bolometric star formation rate shown in Section 2.1.4. This study carried out FUV data photometry using the same method as that for the cluster spiral galaxies.

[10] The field sample galaxies used are NGC 0628, NGC 2841, NGC 2903, NGC 3184, NGC 3198, NGC 3351, NGC 3521, NGC 4736, NGC 5055, NGC 6946, and NGC 7331.

[11] We used the *K*-band total magnitude from 2MASS (Jarrett et al. 2003) for all of the cluster sample galaxies as well as field sample galaxies. For low surface brightness galaxies, 2MASS systematically underestimates their luminosities, especially $m_K > 10$ (Noordermeer & Verheijen 2007). Since LSB galaxies are mainly found among low-luminosity systems at the late-type end of the Hubble sequence, this may also introduce spurious correlations of $L_{\rm CO}/L_K$ with luminosity, size, and Hubble type. However, as seen in Figure 3, the sample galaxies in this study spans a range of morphological types of Sa–Scd and a *K*-band magnitude (m_K) of less than 9.5 mag for all galaxies except 11 Pisces spiral galaxies. Hence, we can argue that the 2MASS *K*-band luminosity used in this study is reliable. For the Pisces sample galaxies, it is worth noting that the L_K from the 2MASS could be underestimated, and therefore $L_{\rm CO}/L_K$ overestimated.

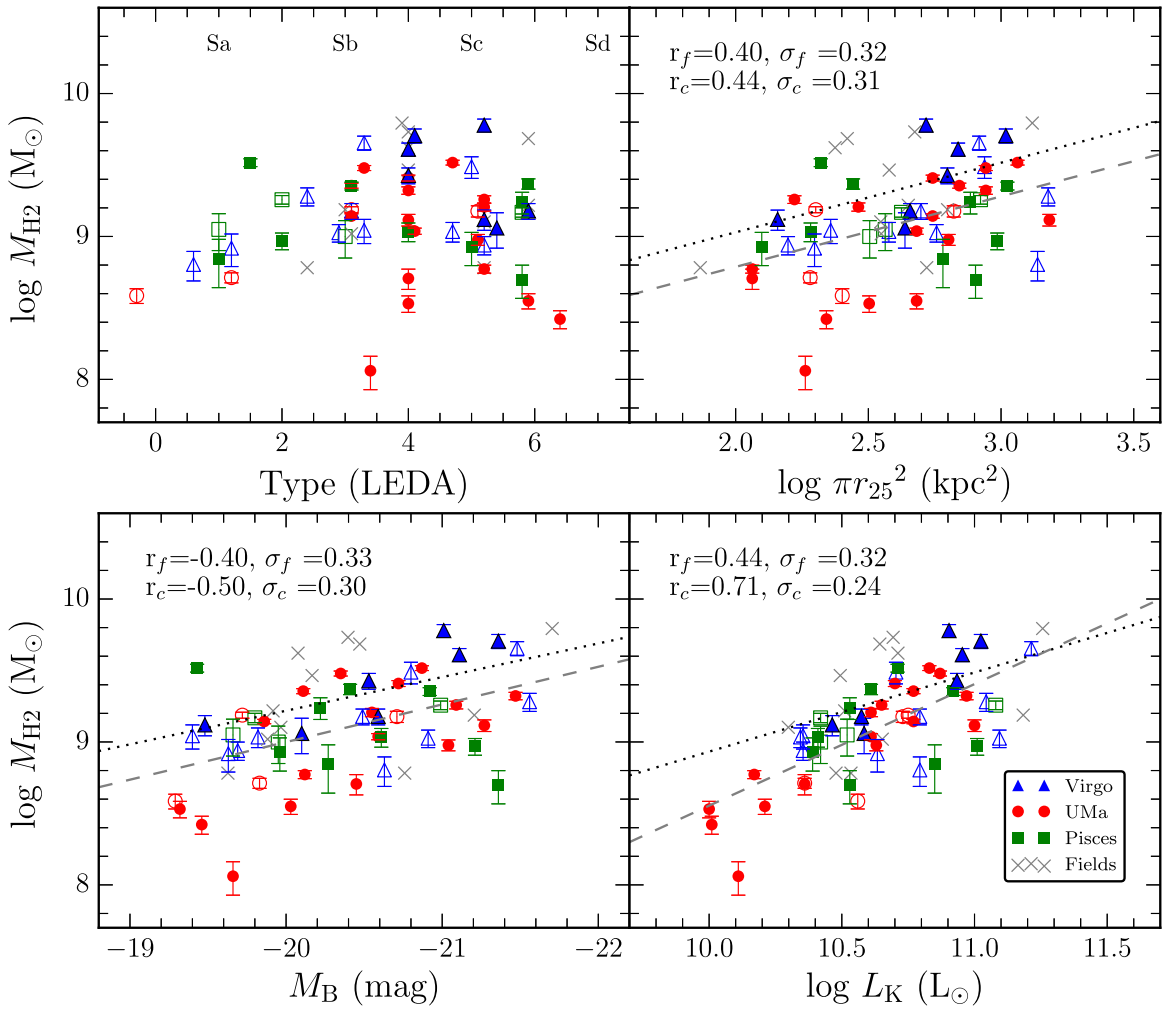

Figure 4. Molecular gas mass derived with constant X_{CO} as a function of the morphological type (top left), the optical surface area (top right), the corrected optical *B*-magnitude (bottom left), and the *K*-band luminosity (bottom right). The Virgo, Ursa Major, and Pisces spiral galaxies are denoted with the blue triangles, red circles, and green rectangles, respectively. The field spirals are denoted with crosses. The open and solid symbols present the H I deficiency larger and smaller than 0.4 (i.e., H I deficient and H I normal), respectively. The dotted and dashed solid lines are the least-squares fitting of each relation of the field spiral galaxies and that of cluster spiral galaxies, respectively. The Pearson correlation coefficients (r) and standard deviations from the best-fitting line (σ) for the field (subscript f) and cluster sample spirals (subscript c) are given on the top-left corner in each relationship.

The basic properties of the sample galaxies are shown in Figure 3. The selection criteria used in this study tend to choose galaxies with a large optical diameter and bright in the FIR and/or CO, and the final sample could omit galaxies that are severely depleted in CO. However, the Virgo cluster sample includes highly H I-stripped galaxies and the other sample consisting of 21 UMa, 13 Pisces, and 11 field spiral galaxies spans a range of morphological type, optical diameter, and *K*-band luminosity similar to the 17 Virgo spiral galaxies. Hence, they can be used to investigate the CO properties of the galaxies in the various environments.

3. CO Properties in Different Environments

3.1. CO Properties as a Function of the Optical Parameters

Before the molecular gas properties are investigated with the cluster environments, the properties of the molecular gas with the optical properties of the galaxies were examined. This is indispensable in order to minimize the possibility of confusing the properties of the innate molecular gas with the environmental effects. The general properties of the molecular gas as a function of the morphological type (numerical morphological type code from LEDA), the optical size defined at the 25th magnitude per square arcsec in the *B*-band (LEDA), the absolute *B*-band magnitude (LEDA), and the *K*-band luminosity (2MASS; Jarrett et al. 2003) are shown in Figure 4. The Virgo, UMa, and Pisces spiral galaxies are denoted with triangles, circles, and squares, respectively. H I-deficient galaxies ($def_{H\,I} > 0.4$) and H I-normal galaxies ($def_{H\,I} \leqslant 0.4$) are indicated with open and solid symbols, respectively. Field comparison samples are denoted with gray crosses.

As shown in the top-left panel of Figure 4, galaxies with a high H_2 mass ($M_{H2} > 3 \times 10^9\,M_\odot$) are mostly Sb–Sc; however, generally, no noticeable trend is found between the molecular gas mass and the morphological type. Galaxies with a low H_2 mass are also found among all types. The independence of the molecular gas mass from the morphology is consistent with many previous studies (e.g., Young & Scoville 1991; Lisenfeld et al. 2011; Boselli et al. 2014a, 2014b, 2014c).

As shown in the top-right panel, the molecular gas mass has an extremely weak correlation with the optical surface area. There is, however, quite a large scatter in this relation, and the molecular gas mass ranges widely for the given optical size measured in the *B*-band. The *B*-band magnitude shows the

same trend in the sense that the overall molecular gas mass increases with increasing luminosity but the scatter is quite large (>1 dex).

On the other hand, the molecular gas mass is found to be tightly correlated with the *K*-band luminosity—a proxy of the stellar mass of galaxies ($r = 0.66$ and $\sigma = 0.27$ for the entire sample and $r = 0.71$ and $\sigma = 0.27$ for the H I-normal galaxies). In fact, Boselli et al. (2014a, 2014b, 2014c) also showed that the galaxy size measured at a longer wavelength (e.g., the *g*-band) and the stellar mass estimated using the *i*-band luminosity and the *g*– *i* color-dependent stellar mass-to-light ratio correlate well with the molecular gas mass.

This study presents the least-squares fitting of the field and cluster spiral galaxies for each relationship. In the log M_{H2}–log πr_{25}^2 and log M_{H2}–M_B relationships, the field galaxies have a slightly larger M_{H2} than that of the cluster spiral galaxies (average log $M_{H2} = 9.31 \pm 0.37$ for the field and 9.08 ± 0.35 for the cluster galaxies); however, the slopes are not that different between the cluster and field spiral sample galaxies. In the log L_K relationship, there exists a trend that the difference in the molecular gas mass between the field and cluster galaxies becomes smaller as the galaxy becomes brighter in the *K*-band. The difference in the molecular gas mass between the field and cluster galaxies is ∼0.4 dex for the smallest L_K but almost zero for the largest L_K. This difference is not significant considering the large scatter of the molecular gas mass in the sample used in this study. Hence, it can be concluded that the molecular gas mass of the cluster galaxies has hardly any distinct correlation with the optical properties from that of field galaxies.

The following summarizes the relations between the molecular gas mass and the general optical properties:

1. Molecular gas mass does not strongly depend on the morphological type.
2. Molecular gas mass shows weak correlations with *B*-band optical size and luminosity; however, the scatter is large, and the molecular gas mass is widely distributed for a given *B*-band size or luminosity.
3. Molecular gas mass tightly correlates with the *K*-band luminosity, i.e., the stellar mass of the galaxies.
4. The relationships of the molecular gas mass and the optical properties have similar slopes in all environments although the cluster galaxies have a slightly lower M_{H2}.

To compare the molecular gas properties of spiral galaxies in different environments, galaxy size should be taken into account. M_{H2} correlates tightly with L_K for the field sample in the limited number of cases used in this study (Figure 4) but is also shown with a large sample by Gavazzi et al. (1996), and the L_{CO}/L_K or M_{H2}/L_K ratios can be a reasonable quantity to use in the investigation of the molecular gas content of galaxies in different environments not affected by the size effect.

3.2. CO Luminosity and H I Deficiency

This section examines the relationship between the CO luminosity normalized by the *K*-band luminosity and H I deficiency $def_{H\,I}$, which is an effective measure of the impact of the environment, as discussed in Section 2.1.3. H I gas is generally the most vulnerable component in a galaxy because it extends well beyond the optical size (∼2 times; e.g., Hewitt et al. 1983), and thus gravitationally weakly bound. Hence, it is easily affected by any external forces and often serves as a useful tool to investigate how galaxies interact with their surroundings (e.g., Hibbard et al. 2001; Chung et al. 2009a). Comparing the molecular gas content of galaxies with their H I deficiency may provide useful insight into the severity of the impact of the environmental factors on the inner depth of the gas disks.

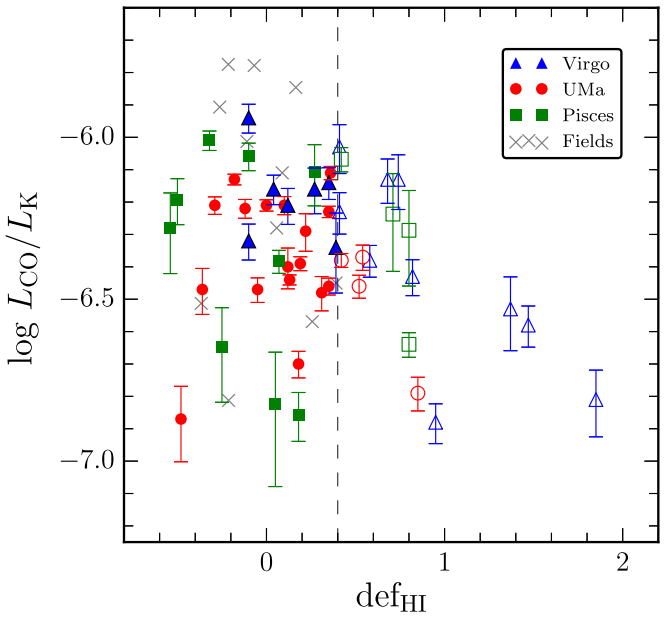

Figure 5. H I deficiency vs. the log of the CO luminosity normalized by the *K*-band luminosity. Symbols are as in Figure 4.

Figure 5 shows the L_{CO}/L_K ratio of the entire sample as a function of the H I deficiency, $def_{H\,I}$. The most severely H I-stripped galaxies with a $def_{H\,I}$ of ∼1–2 (e.g., $M_{H\,I}$, 10–100 times smaller compared to the field counterparts) are found only in the Virgo cluster while the UMa and Pisces cluster galaxies, at most, show only a modest H I deficiency. Intriguingly, the L_{CO}/L_K ratio appears to decrease with an increasing $def_{H\,I}$ for the Virgo sample, which may indicate that H I-deficient galaxies are also deficient in molecular gas. However, the remaining UMa, Pisces, and field sample galaxies span nearly the same range of the L_{CO}/L_K ratio, i.e., a comparable number of galaxies that are normal in H I are found to have as low a CO content as the severely H I-stripped galaxies. Boselli et al. (2014a, 2014b, 2014c) also show the presence of galaxies with a normal H I but with a deficient H_2, and they attribute it to the large uncertainties.

Figure 6 shows the histograms of the CO luminosity normalized by the *K*-band luminosity for the H I-normal (top) and H I-deficient (bottom) galaxies for all (clusters and fields), Virgo, UMa, and Pisces cluster sample galaxies. The L_{CO}/L_K ratio for the H I-normal spiral galaxies of the whole sample spans a range between −7 and −5.7 (in log scale) with a fairly symmetric log-normal distribution with a median value of −6.25 in log scale. In comparison, the L_{CO}/L_K ratio distribution for the H I-deficient spirals has a slightly low peak (the median value of −6.4 in log) and is skewed to the left because of the absence of a high L_{CO}/L_K ratio wing and also a higher portion of the lowest L_{CO}/L_K ratio.

The three right panels of Figure 6 represent well the distinction of the gas component in each cluster. The first one is

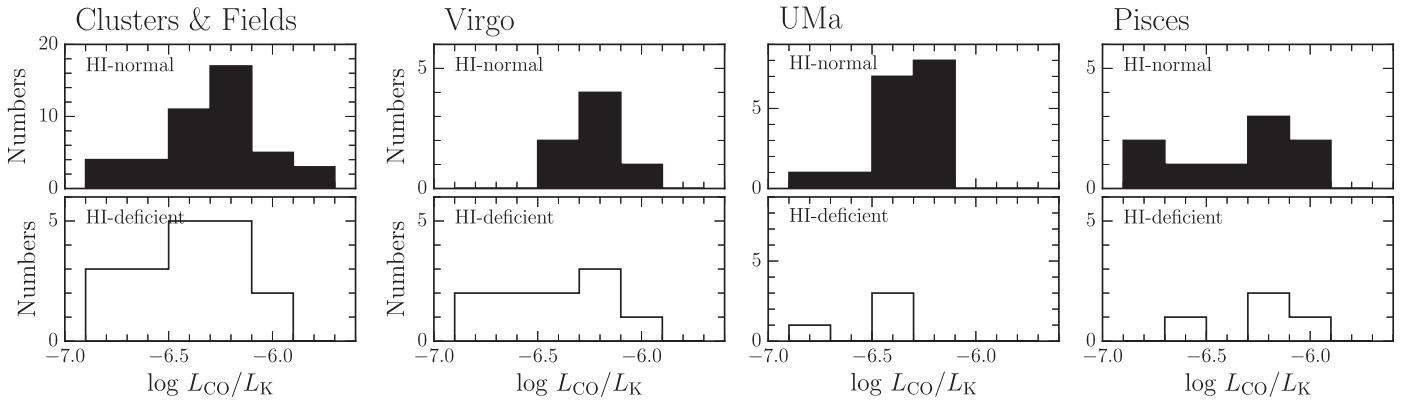

Figure 6. Different distributions of the log L_{CO}/L_K of the H I-normal and H I-deficient galaxies.

that while H I-depleted galaxies are dominant in the Virgo cluster sample, H I-normal galaxies are primarily in the UMa and Pisces cluster sample spiral galaxies. This is predictable because the Virgo has a hot ICM in the cluster center, and the probability of H I stripping is high due to the interaction with the ICM, but the UMa and Pisces clusters do not have a hot ICM in the cluster center.

Second, the distribution of L_{CO}/L_K is clearly different between the H I-normal and H I-deficient galaxies in the Virgo cluster. The L_{CO}/L_K ratio of the H I-normal galaxies is in the range of -6.5 and -5.9 in log scale, but that of the H I-deficient galaxies is spread out to a much lower value (~ -6.9 in log). This low end of L_{CO}/L_K is because of those galaxies that are highly stripped in H I ($\mathrm{def}_{H\,I} \gtrsim 0.8$), shown in Figure 5. In contrast, the UMa and Pisces samples do not show such a clear difference in L_{CO}/L_K between the H I-normal and H I-deficient galaxies. For the UMa spirals, H I-deficient galaxies tend to have a slightly lower L_{CO}/L_K than H I-normal galaxies, although it is not as significant as the Virgo spirals. For the Pisces cluster spirals, there is no discrepancy in L_{CO}/L_K between the H I-normal and H I-deficient galaxies. This can be due to the lack of severely H I-stripped galaxies in the UMa and Pisces clusters. However, it could be worth noting that these two clusters have galaxies for which the H I content is normal, but L_{CO}/L_K is as low as that of the highly H I-stripped Virgo galaxies.

3.3. CO Diameter in Different Environments

Here, the CO and H I isophotal diameters (D_{CO}^{iso} and $D_{H\,I}^{iso}$) are examined as possible indicators of influence from the environment. CO and H I isophotal diameters are defined by the area where the mean face-on surface density of H_2 and H I falls to 1 $M_\odot\,pc^{-2}$. H_2 surface density distributions (in units of $M_\odot\,pc^{-2}$) are derived from the CO radial distribution assuming a constant CO to H_2 conversion factor. Pisces spiral galaxies that are not fully mapped in CO were excluded in this analysis.

In deriving a radial density profile, a concentric ellipse-fitting method does not work well for the CO data used in this study due to the large beam size. Hence, the CO radial distributions of the Virgo and UMa samples were derived following Warmels (1988). To derive the H I diameters of the Virgo spirals, moment 0 maps from the VIVA survey are smoothed to a 45″ resolution to match the CO resolution, and the H I radial distributions are derived following Warmels (1988). The $D_{H\,I}$ of the UMa spiral galaxies are taken from Verheijen & Sancisi (2001). For the field spiral galaxies, this study used the H I and CO moment 0 maps from the THINGS and HERACLES surveys. Likewise, the $D_{H\,I}$ and D_{CO} for the field sample galaxies were derived from their radial distributions after degrading the data to a 45″ resolution.

In Figure 7, the CO diameters are compared with the H I and optical diameters. For the majority of the galaxies shown, the H I extends out to 1.5–2 times that of the stellar diameter while some (mostly Virgo) cluster spirals with a truncated H I disk ($D_{H\,I}/D_{opt} < 1$) are also present. As for the CO, a previous study analyzing a much larger sample by Young et al. (1995) reported that the CO diameter typically extends to about half the optical diameter. The CO diameters of the sample in this study also range between 0.5 and ∼1 optical diameter (see the left panel), and there seems to be a tight correlation between the CO and H I diameters with a systematic increase in the D_{CO}/D_{opt} ratio with the increasing $D_{H\,I}/D_{opt}$. This trend disappears at $D_{H\,I}/D_{opt} > 2$. The Virgo spirals with a truncated H I disk ($D_{H\,I}/D_{opt} < 1$) approximately follow the $D_{CO} = D_{H\,I}$ line shown with a solid line.

The right panel of Figure 7 shows the comparison between the CO and H I diameters again but with $D_{CO}/D_{H\,I}$ as a function of $D_{H\,I}/D_{opt}$. The ratio between the CO to H I diameter for those galaxies with a H I disk size between ∼1.5 and 3 D_{opt} shows a slightly decreasing tendency with increasing $D_{H\,I}/D_{opt}$ but remains fairly constant (∼0.3–0.5). However, the H I-deficient Virgo and UMa spirals show a sharply increasing $D_{CO}/D_{H\,I}$ ratio toward unity as the $D_{H\,I}/D_{opt}$ ratio decreases from ∼1.5 to 0. This trend is pretty tight and obvious despite the large uncertainties in these ratios.

It is interesting that spiral galaxies in various environments follow the same trend as the D_{CO} and $D_{H\,I}$ relation, and two things can be inferred about the characteristics of the CO and H I distribution. First, the same trend of the diameter of the molecular gas and that of the atomic gas relation regardless of the environment suggests that the extent of the molecular gas is under the control of the atomic gas distribution as well as the depth of the gravitational potential well characterized by its optical size. Bigiel & Blitz (2012) claim that a universal radial gas profile is driven by the stellar mass distribution in nearby spiral galaxies. Meanwhile, theoretical models suggest that the molecular gas fraction in a galaxy is determined by its column density and metallicity and by the strength of the interstellar

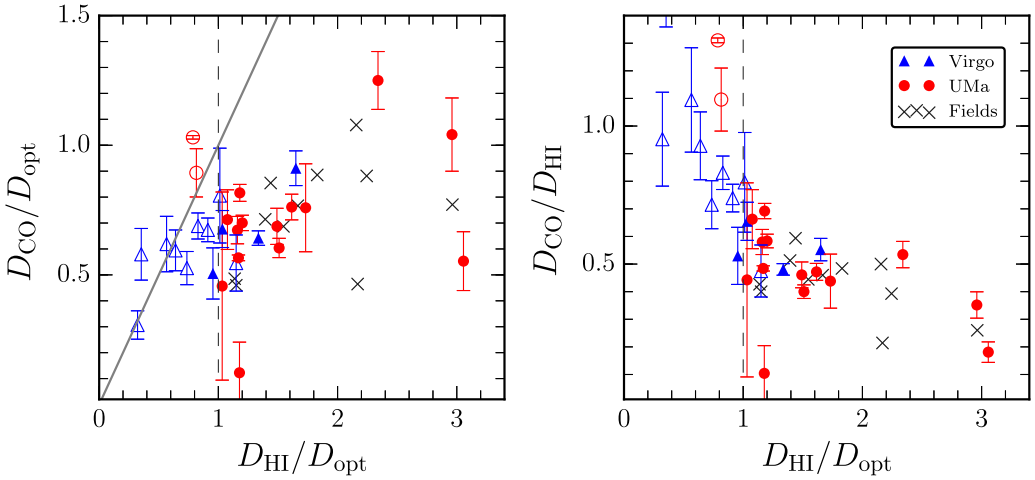

Figure 7. (Left) Comparison of the CO and H I diameters normalized by the optical diameters. (Right) Ratio of the CO to H I diameters with the H I to optical diameter ratios. The dashed and solid lines represent the $D_{H\,I} = D_{opt}$ and $D_{CO} = D_{H\,I}$ relations, respectively. Only the errors in CO measurements are shown since the H I and optical errors are not available for the entire sample. The uncertainties in the H I diameters are small compared to the uncertainties in the CO diameters for the cases with known uncertainties, and this seems true for nearly all cases based on the spatial resolution and the quality of the data used.

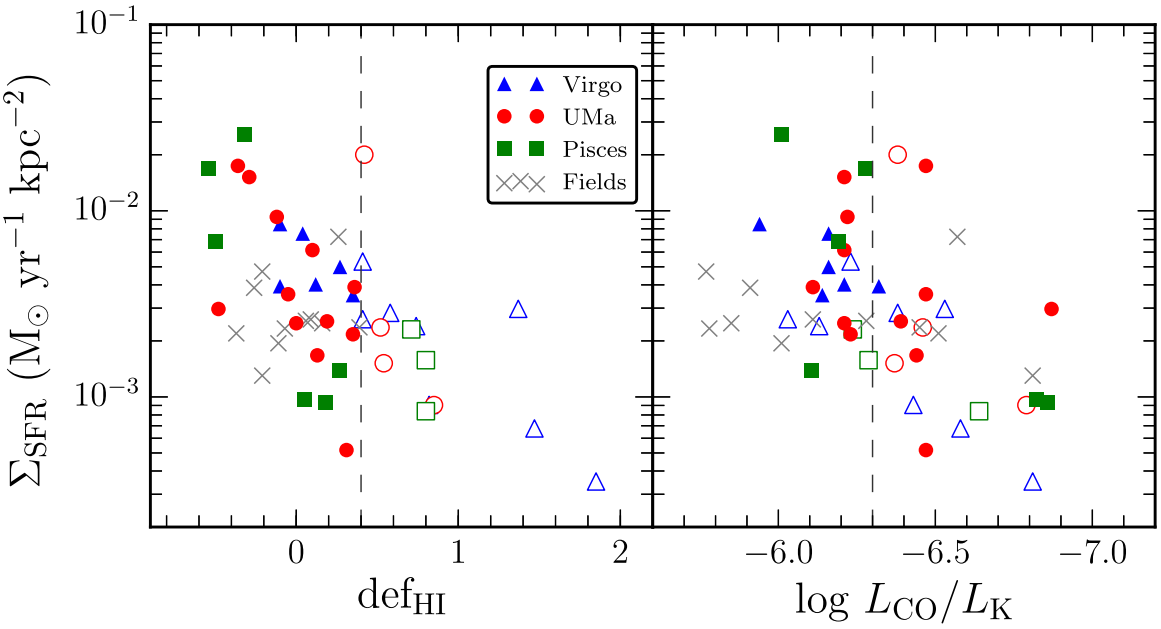

Figure 8. Comparisons of the disk-averaged SFR per unit area (Σ_{SFR}) of galaxies with the H I deficiency (left panel) and normalized CO luminosity (right panel). Symbols are as in Figure 4.

radiation field (Krumholz et al. 2009a, 2009b). The linear correlation of the CO and H I diameters shown in the sample of this study strongly supports these two predictions.

Another inference one can make from these analyses is that the depletion of the molecular gas by the intracluster medium among the Virgo and UMa spirals with a truncated H I disk is a gradual (rather than a sharp, threshold-driven) process. Boselli et al. (2014a, 2014b, 2014c), who used the same CO and H I data for the Virgo spirals as in this study and hence showed the same trend for the CO and H I extents as a function of the $def_{H\,I}$, also concluded that the removal of molecular gas by ram pressure is less efficient than the removal of atomic gas. Inclusion of the UMa and field samples makes this clearer. If molecular gas is simultaneously stripped away by ram pressure along with atomic gas, the $D_{CO}/D_{H\,I}$ ratio is expected to change abruptly to ~1. Instead, the trend seen in the right panel of Figure 7 is smooth and continuous, suggesting a more gradual process for the removal of molecular gas with respect to atomic gas.

4. Star Formation Rate

4.1. Star Formation Rates and Gas Properties

To investigate the star formation activity of spiral galaxies in different cluster environments, this study examined the total bolometric star formation rates ($SFR_{tot} = SFR_{FUV} + SFR_{FIR}$, Section 2.1.4). The disk-averaged SFR per unit area ($\Sigma_{SFR} = SFR_{tot}$/disk area) is represented as a function of the $def_{H\,I}$ and log L_{CO}/L_K shown in Figure 8. The field galaxies show $\Sigma_{SFR} \sim 10^{-3}$–$10^{-2}\,M_\odot\,yr^{-1}\,kpc^{-2}$. In comparison, the

$\Sigma_{\rm SFR}$ of the cluster sample ranges between 3×10^{-4}–$3 \times 10^{-2}\,M_{\odot}\,{\rm yr}^{-1}\,{\rm kpc}^{-2}$ with a large scatter.

Leroy et al. (2008, hereafter L08) obtained a resolved $\Sigma_{\rm SFR}$ based on the *GALEX* FUV and *Spitzer* 24 μm maps for 23 nearby late-type galaxies, and its range is between 10^{-4} to $10^{-1}\,M_{\odot}\,{\rm yr}^{-1}\,{\rm kpc}^{-2}$. The difference in the $\Sigma_{\rm SFR}$ between this study's and L08's sample may be caused by the difference in the integrated and resolved SFR. The $\Sigma_{\rm SFR}$ of L08 is much broader than the disk-averaged $\Sigma_{\rm SFR}$ of the field sample in this study because L08 includes the highest $\Sigma_{\rm SFR}$ (generally in the galactic center) and also the lowest $\Sigma_{\rm SFR}$ (in the outer disk) while this study has a single value for the $\Sigma_{\rm SFR}$ for the entire galaxy. Another reason that could cause the variation between the two $\Sigma_{\rm SFR}$ is the use of different star formation indicators. Comparing the integrated SFR within $1.5r_{25}$ of L08, the SFR in this study derived with the FUV and *IRAS* 60 and 100 μm is well matched with L08's SFR calculated with the FUV and MIPS 24 μm. However, for three galaxies (N3521, N5055, and N6946), this study has a lower SFR than L08 by a factor of two, and this may cause the large scatter in the $\Sigma_{\rm SFR}$ (and also in the gas consumption time in the next section).

There are two notable things seen in the comparison of the $\Sigma_{\rm SFR}$ and gas properties shown in Figure 8. The first one is the linear correlations between the $\Sigma_{\rm SFR}$ and gas contents of the cluster galaxies. Galaxies with a high star formation rate are mostly found among the H I-normal/rich population while H I-poor galaxies show diminished star formation activity on average. This is only a weak trend and is expected for the H I-deficient galaxies with a truncated gas disk because the areas of star formation activity is reduced compared with the overall extent of the stellar disk (e.g., Koopmann & Kenney 2004a, 2004b). The right panel of Figure 8 shows that galaxies with a low CO content ($\log L_{\rm CO}/L_{\rm K} < -6.3$) have a smaller average $\Sigma_{\rm SFR}$ than the galaxies with $L_{\rm CO}/L_{\rm K} > -6.3$ in log. The other one is that the field galaxies do not follow the trend seen in the cluster galaxies. In particular, as seen in the right panel of Figure 8, the decreasing trend of $\Sigma_{\rm SFR}$ as $\log L_{\rm CO}/L_{\rm K}$ decreases does not hold for the field galaxies, which span the full range of $\log L_{\rm CO}/L_{\rm K}$. Using L08's $\Sigma_{\rm SFR}$ instead of the one in this study makes the difference between the cluster and the field sample decrease; however, the field sample is still distinguished from the cluster sample (slopes of the $\Sigma_{\rm SFR}$ and $\log L_{\rm CO}/L_{\rm K}$ relationship are 0.0084 for the cluster and 0.0010 for the field with this study's $\Sigma_{\rm SFR}$ and 0.0059 for the field with L08's $\Sigma_{\rm SFR}$). This can be a relevant result, which suggests that the relation between the SFR and the H_2 content of galaxies is dependent on the environment.

4.2. Gas Consumption Time

The time it takes a galaxy to consume all of its cool gas by star formation can be computed using the current gas mass and star formation rate as follows:

$$t^{\rm gas}({\rm year}) = \frac{M_{\rm gas}(M_{\odot})}{{\rm SFR}(M_{\odot}\ {\rm yr}^{-1})}, \quad (7)$$

where SFR is the star formation rate and $M_{\rm gas}$ is the H I, H_2, and total gas mass, which does not include a correction for helium mass. Figure 9 shows the atomic and molecular hydrogen gas and total gas consumption times as a function of $\rm def_{H\,I}$ and $L_{\rm CO}/L_{\rm K}$. The range for the atomic and molecular gas consumption times of the cluster galaxies is between 0.2–10 Gyr and 0.2–4 Gyr, respectively. The field sample has slightly longer atomic and molecular gas consumption times than the cluster sample ($t^{\rm H\,I} \sim 0.6$–10 Gyr and $t^{\rm H2} \sim 0.5$–5 Gyr).

L08 reported that the nearby spiral galaxies have an almost constant $t^{\rm H2}$ of ~1.9 Gyr, which is similar to the mean $t^{\rm H2}$ of the field sample galaxies in this study. The COLD GASS sample shows broad ranges for the gas consumption time ($t^{\rm H\,I} \sim 0.3$–30 Gyr and $t^{\rm H2} \sim 0.3$–3 Gyr), which is selected strictly by the stellar mass and is independent of the environment (Saintonge et al. 2011b). Bigiel & Blitz (2012) found an approximately constant $t^{\rm H2}$ of ~2.3 Gyr, for which the helium mass fraction was considered in the nearby disk galaxies. Without the helium mass fraction, it is ~1.8 Gyr and is approximately the same in the field and H I-stripped spiral samples used in this study. Boselli et al. (2014a, 2014b, 2014c) provided an average $t^{\rm H2}$ of ~0.6 Gyr and $t^{\rm H\,I+H2}$ of ~4.0 Gyr for gas-rich galaxies ($\rm def_{H\,I} \leqslant 0.4$) and $t^{\rm H2}$ of ~1.2 Gyr and $t^{\rm H\,I+H2}$ of ~2.6 Gyr for H_2-deficient cluster galaxies with the *Herschel Reference Survey* sample. Mok et al. (2016) obtained a mean $t^{\rm H2}$ of ~0.9 Gyr and 0.3 Gyr for the Virgo and the group samples, respectively.

As shown in the top-left panel of Figure 9, the atomic gas consumption time is inversely proportional to the H I deficiency. Although both the star formation rate and the atomic gas mass tend to be smaller in H I-deficient galaxies, losing H I gas appears to have a stronger impact leading to the observed anti-correlation between the atomic gas consumption time and the H I deficiency. These trends are somewhat expected because gas stripping precedes star formation quenching.

In contrast, the molecular gas consumption time seems to *increase* with the H I deficiency, especially among galaxies in the same cluster. The galaxies in each cluster show a consistent pattern of an increasing $t^{\rm H2}$ with $\rm def_{H\,I}$ spanning the full range of $\rm def_{H\,I}$. These cluster galaxies are distinct from the field sample in that their molecular gas consumption times are up to an order of magnitude smaller. As addressed in the previous section, the use of the *IRAS* FIR data set can cause a large scatter in the molecular gas depletion time, too. However, this study found that even L08's SFR from Hα and MIPS 24 μm makes a clear difference in $t_{\rm H2}$ (~0.6–2.5 Gyr) from that of the H I-normal cluster sample. The comparison sample of the field galaxies appears to have a slightly higher mean $L_{\rm CO}/L_{\rm K}$ ratio compared with the cluster galaxies in Figure 5 while they have a slightly lower mean SFR in Figure 8. Both of these effects are only marginally significant individually. The gas consumption time combines these two effects together, leading to a clearer separation of the field sample from the cluster sample in Figure 9.

Although rarely noticed in previous studies, this trend of accelerated gas consumption in cluster galaxies may be a different realization of the more familiar concept of "pre-processing," which is thought to occur in galaxies in a group environment prior to entering the cluster potential (e.g., Zabludoff & Mulchaey 1998; Kodama et al. 2001; Odekon et al. 2017). There are plenty of studies showing that tidal interaction in modest overdensity leads to enhanced star formation activity, and thus preprocessing. Most recently, Cao et al. (2016) observed 88 *K*-band selected major-merger galaxy pairs (H-KPAIRs) with *Herschel* and found a significantly enhanced specific SFR (sSFR) and SFE in

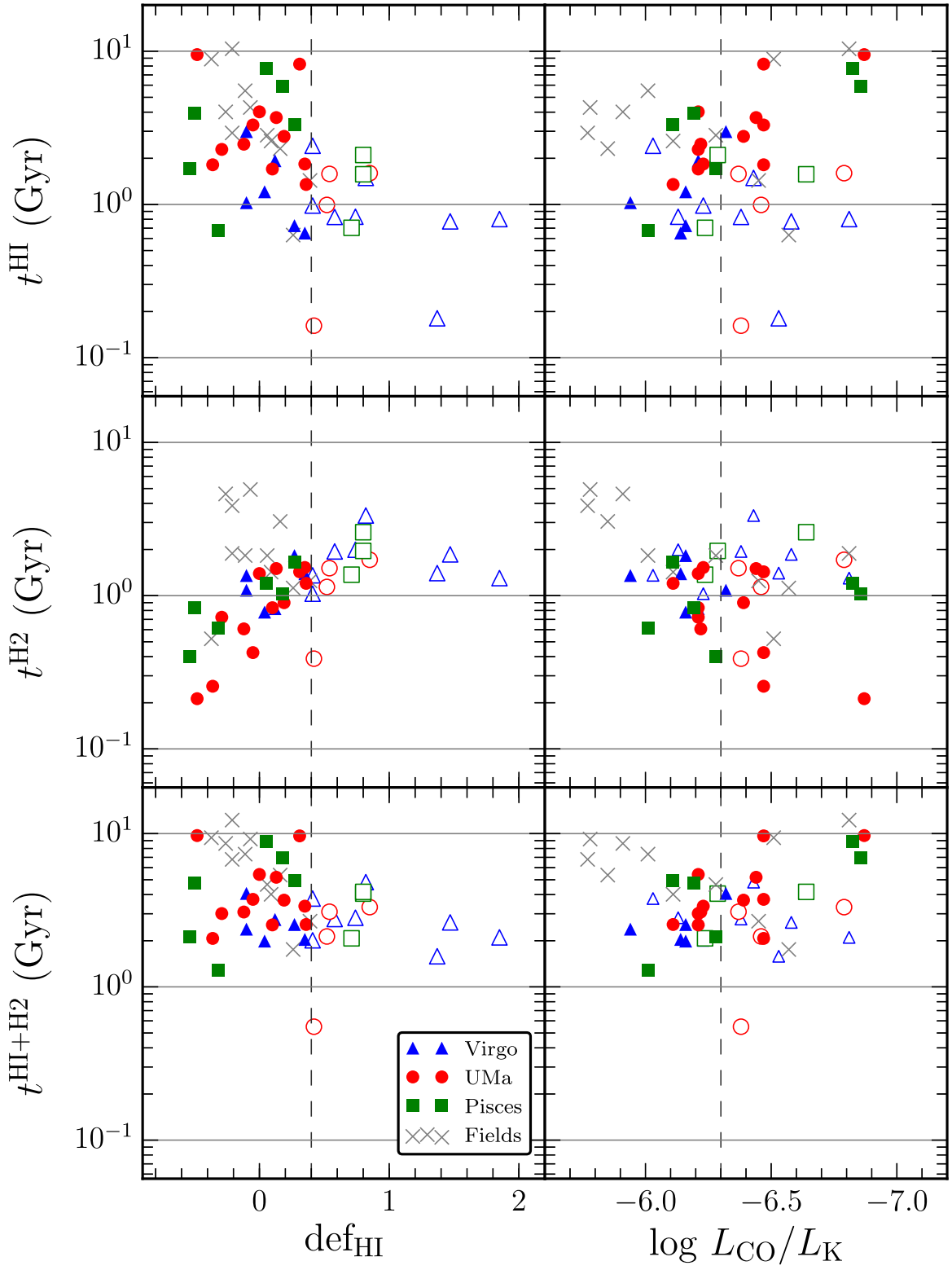

Figure 9. Gas consumption times for the H I mass ($t^{\rm H\,I}$), H_2 mass ($t^{\rm H2}$), and total gas mass ($t^{\rm H\,I+H2}$). Symbols are identical to those in Figure 4.

spiral−spiral pairs. Additionally, the enhanced sSFR and SFE are not different between the galaxy pairs with and without interaction signs. The same galaxies have been observed with the Green Bank Telescope (GBT), and one of the main conclusions is the $\rm SFE^{H\,I}$ is enhanced among these mass-selected pairs, meaning star formation is enhanced without affecting the H I content (P. Zuo et al. 2017, in preparation). It is well established that the H I content is extremely insensitive to both gas accretion and star formation. As Putman et al. (2012) and others have shown, the H I around

galaxies is not the external gas reserve that fuels the molecular gas in the disk but a transitional phase between the larger halo and the cold ISM in the center. Recent papers on cosmological stellar mass build-up and gas content by Genzel et al. (2015) and Scoville et al. (2016, 2017) all show the same picture that the order of magnitude change in specific SFR at a given stellar mass along the main sequence over cosmic time is driven by the corresponding changes in the molecular gas mass fraction while the atomic gas content is insignificant and relatively constant over cosmic time (except for the very recent past). Thus, it is likely that the only place where H I content is significantly different is in the cluster cores where RPS is cutting off the gas infall from the halo. In this scenario, one would expect the H I content to be relatively insensitive to the enhanced star formation activities due to tidal interactions.

Highly H I-deficient galaxies are lower in both molecular gas content and star formation activities, and their offsetting effect on the molecular gas consumption time results in values similar to those of the field sample. Consequently, the t^{H2} of the H I-stripped galaxies ($def_{H\,I} > 0.4$) is slightly higher than that of the cluster galaxies with a normal H I content. Mok et al. (2016) have reported similar results, showing that the molecular gas depletion times of the Virgo spirals are longer compared to those of the galaxies in the group environment. Boselli et al. (2014a, 2014b, 2014c) also show that H I-deficient galaxies have a longer molecular gas consumption time than H I-normal galaxies.

The total cool gas ($H\,I + H_2$) consumption time is more uniform for the entire sample, with a slight trend for decreasing gas consumption time with increasing $def_{H\,I}$. On average, the field sample has a slightly larger total cool gas consumption time compared with the cluster galaxies, while the H I-deficient and H I-normal cluster galaxies have a similar total gas consumption time. This relative insensitivity of the total cool gas consumption time compared with the spread in the total cool gas mass or SFR may reflect the highly local and short timescales associated with the star formation activity (e.g., Boissier et al. 2012; Nehlig et al. 2016). A more prominent trend associated with the molecular gas consumption time compared with the atomic or total gas consumption time suggests that an internal process such as a tidally induced inflow or harassment is more important than external, ICM-driven processes such as ram pressure (except for severely H I-deficient galaxies) or strangulation to account for the overall observed trends here.

4.3. Effects of the Environment on Molecular Gas

Atomic gas, the reservoir for future star formation, is constantly replenished by accretion processes, and this complicates the picture of H I deficiencies: atomic hydrogen can be actively removed from galaxies through ram-pressure and/or tidal stripping; however, it can also be depleted by halting the accretion process, which may be relevant during preprocessing. Comparison of global and spatially resolved H I and CO in various environments is necessary; however, data on the molecular gas content of cluster galaxies is sparse, and the impact of the cluster environment on molecular gas is poorly constrained and is still debated. Hence, the main focus of this study was to examine the molecular gas content of a sample of cluster galaxies and the impact of their environment.

Several CO studies on the molecular gas properties of spiral galaxies and the influence of their environment, particularly by the ICM pressure, are found in the literature (e.g., Fumagalli et al. 2009; Scott et al. 2013; Boselli et al. 2014a, 2014b, 2014c). Boselli et al. (2014a, 2014b, 2014c) have recently introduced the H_2-deficiency parameter to explore the impact of the environment. By analyzing the CO data for the *Herschel Reference Survey* sample, Boselli et al. (2014a, 2014b, 2014c) have shown a weak correlation between the molecular gas deficiency and atomic gas deficiency and suggested that molecular gas can be also stripped away by ram pressure.

In this study, the analysis of the global molecular gas content of spiral galaxies in three nearby clusters with different density environments (along with a sample of field spirals) shows that the L_{CO}/L_K ratio spans a wide range of values regardless of the environments or H I deficiency. Cluster spiral galaxies, especially H I stripped by ICM, appear to have a lower L_{CO}/L_K ratio than field spiral galaxies on average—the average L_{CO}/L_K of the H I-deficient galaxies is 0.54 ± 0.04 times lower than that of their comparison field spirals. This study also found that the CO and H I diameters of *all* of the spirals are closely correlated with each other, as expected, if both the atomic and molecular ISM are physically linked with the stellar disk. However, this correlation is not linear, and the ratio of the CO to H I diameter increases as the atomic to stellar disk diameter ratio shrinks, possibly as a result of H I disk truncation induced by their environment. These results suggest that molecular gas can be depleted by the influence of the cluster environment, but the overall impact on the molecular gas is not as dramatic as for the H I.

The average star formation surface density Σ_{SFR} has more than an order of magnitude scatter, and the strongly H I-deficient galaxies have the lowest Σ_{SFR} as expected—the extent of gas disk and star formation is systematically smaller (e.g., Cortese et al. 2010). A bit more surprising is that the molecular gas consumption time for all cluster galaxies, including those with a normal H I fraction (presumably not yet affected by the ICM), is systematically smaller (0.2–4 Gyr) compared with that for the field sample (0.5–5 Gyr). The most H I-deficient cluster galaxies actually have a slightly longer molecular gas consumption time (1–2 Gyr), suggesting this accelerated processing of gas into stars is not directly related to global cluster effects such as ram pressure or strangulation. Rather, it is likely related to the higher galaxy density of the large-scale structure surrounding the clusters, such as tidally induced activities (e.g., Verdes-Montenegro et al. 1998; Verheijen 2004; Cybulski et al. 2014), perhaps similar to the preprocessing phenomenon commonly associated with the group environment. There could be other alternative explanations, such as a lower CO luminosity associated with lower metallicity galaxies still infalling onto the cluster; however, finding the same trend in all three clusters (Figure 9) strongly suggests a common physical mechanism at work. Verifying this trend in a larger sample of cluster galaxies would lead to extremely interesting new insights into the evolution of galaxies in a high-density environment.

5. Summary

This study investigated the environmental effects on molecular gas and star formation activity. In particular, which kind of environmental effect is predominant in which

environment and whether molecular gas also can be removed from galaxies as effectively as H I by mechanisms like ram-pressure stripping were investigated. For this, the CO and star formation properties of 17 Virgo, 21 UMa, and 13 Pisces spiral galaxies as well as 11 field spiral galaxies were examined and compared with their H I data, i.e., the component that clearly shows the environmental effects for both global and radial properties. The CO flux-based global molecular gas properties were examined for the entire sample, while the radial properties were compared just for the Virgo, UMa, and field galaxies because full mapping data are available only for these samples. Among a number of star formation indicators, the total bolometric star formation rates with FUV and FIR were used in this work.

The highlights of this study can be summarized as follows.

1. Log L_{CO}/L_K ranges broadly in all environments, but it does not largely differ as the H I, which covers two orders of magnitude. Additionally, the relative CO content ($\log L_{CO}/L_K$) of H I-stripped galaxies appears to be slightly smaller than that of the field spiral galaxies on average; however, the difference is not obvious (mean $\log L_{CO}/L_K$ is -6.45 ± 0.31 and -6.18 ± 0.36 for the H I-stripped and field sample galaxies, respectively). This suggests that ICM pressure may induce molecular gas deficiency, but even if so, the overall impact must not be as noticeable as the atomic gas deficiency.
2. The increasing trend of D_{CO}/D_{opt} as $D_{H\,I}/D_{opt}$ becomes larger implies that CO can be affected by their environments. However, the constant ratio of CO to the H I diameter for the galaxies that have a H I diameter larger than their optical diameter and for the increment of $D_{CO}/D_{H\,I}$ up to 1 when the atomic gas is stripped inside the optical diameter indicate that the molecular gas supposedly does not respond as immediately as the atomic gas does but gradually to the ICM pressure.
3. Galaxies with low global star formation activity are always poor in H I and/or H_2. The analysis of the gas consumption times in this study suggests that the cluster galaxies may have a different evolutionary track from that of the field sample. Losing cool gas by preprocessing and/or ICM pressure may result in the suppression of star formation, turning a galaxy passive in the cluster environment earlier than in the field.

From the results of this study, it can be concluded that in a high-density region with hot ICM like the Virgo cluster and in a low density galaxy group environment like UMa and Pisces, the depletion of cold gas by ICM pressure and starvation caused by preprocessing, respectively, might be the major processes to determine the evolutionary path and fate of a galaxy. On the other hand, we found some hints that the molecular gas disk shrinks after atomic gas stripping; yet, it is unlikely to be a dramatic change. Even if the global properties of the molecular gas do not get modified significantly, it does not rule out the possibility of a change in the internal properties of the molecular gas. Indeed, a recent high-resolution CO mapping study of a subsample of the Virgo galaxies undergoing strong ram pressure by Lee et al. (2017) clearly shows that the molecular gas morphology can also be modified by the ICM pressure. Therefore, we conclude that the cluster environment, which includes ram pressure, preprocessing, and tidal interaction, can modestly change the molecular gas property, star formation activity, and eventually the evolution of a cluster spiral galaxy.

We thank the referee for the comments and suggestions. We would also like to thank M.Y. Lee and H. Jeong for their kind help in using the Pisces CO data and GALEX data. This work has been supported by the National Research Foundation of Korea grants No. 2011-0014983 and No. 2015R1D1A1A-01060516. Support was also provided by the Center for Galaxy Evolution Research (NRF grant No. 2010-0027910).

Appendix

A.1. CO Data for Pisces Spiral Galaxies

This section presents the CO spectra of the 13 galaxies of the Pisces filament (Figure 10) and tabulates the general CO properties such as the CO flux, molecular gas mass, CO line width, and CO systemic velocity (Table 2). All galaxies have been detected in CO for the first time except for UGC 540 and UGC 556. Eight galaxies with a low signal-to-noise ratio were two-channel Hanning smoothed and then binned to a 21.8 km s^{-1} velocity resolution. The rest of the galaxies were binned to a 10.4 km s^{-1} velocity resolution. The mean rms of the final data set is ~1.6 mK in the T_{mb} scale.

A.2. Comparison with Previous Observations

Among the sample galaxies used in this study, only two galaxies were previously observed and detected in CO by Lavezzi & Dickey (1998, hereafter LD98). In Figure 11, the global CO profiles of UGC 540 and UGC 556 are presented with those from LD98, which were obtained from the NRAO 12 m telescope with velocity resolutions of 42 km s^{-1} and 21 km s^{-1}, respectively. This study and LD98 derived the CO flux with a coherent method, and this study additionally determined the CO line widths and uncertainties following LD98 (Table 3) for comparison.

The global CO profile of UGC 556 in LD98 seems similar to the one in this study. The shape of the profile, especially the CO line widths, is the same within the uncertainty. However, the data in this study show a higher peak intensity than the data from LD98, resulting in a larger total CO flux (~15%), which might be due to the longer integration time used in this study. These differences could be a result of the different integration times. In contrast, the global profile of UGC 540 in this study is quite different from the spectrum of LD98. With a better signal-to-noise ratio than that of LD98, this study obtained a CO emission at a velocity range of 4800 ~ 4900 km s^{-1}, which seems to be missing in observation by LD98. This results in about a 40% difference for the total CO flux and 50% for the line width.

In summary, in the case of UGC 556, we obtained consistent results with LD98. We estimated more reliable CO quantities for UGC 540 than LD98. Thus, we conclude that our observations are more sensitive than those of LD98. However, this comparison with another survey suggests that our observations might have the same systematic errors in cases with a low signal-to-noise ratio. For example, the CO profiles of NGC 452 and UGC 575 are quite noisy and weak. The CO properties of these galaxies should be cautiously used in other applications, and further observations are required.

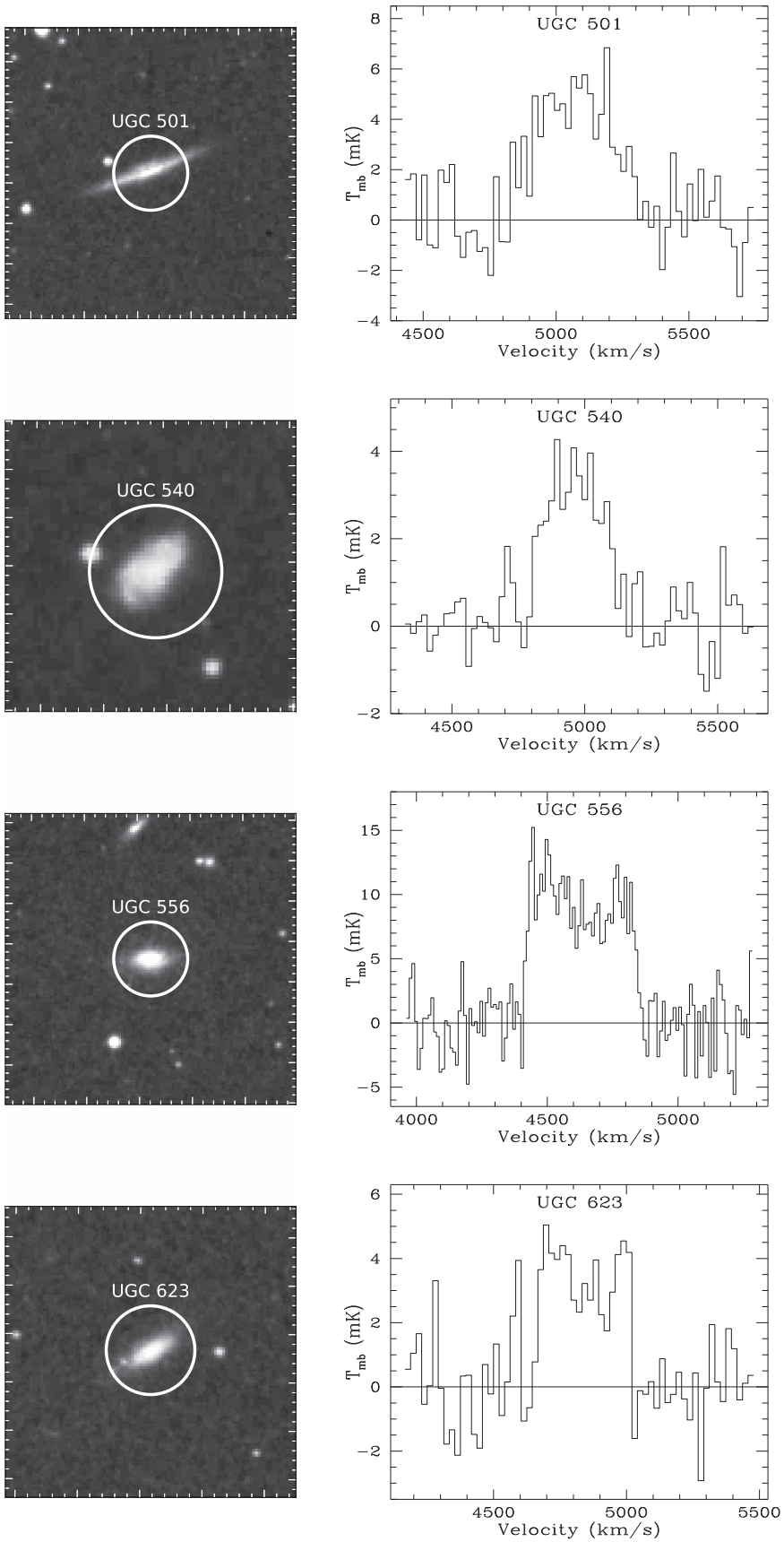

Figure 10. Palomar Sky Survey images (left) and CO spectra (right) of 13 Pisces spiral galaxies. The white circle represents the region covered by the beam of the telescope. The axes of the CO spectra are the main-beam brightness temperature (T_{mb}) in mK and the heliocentric velocity in km s^{-1}.

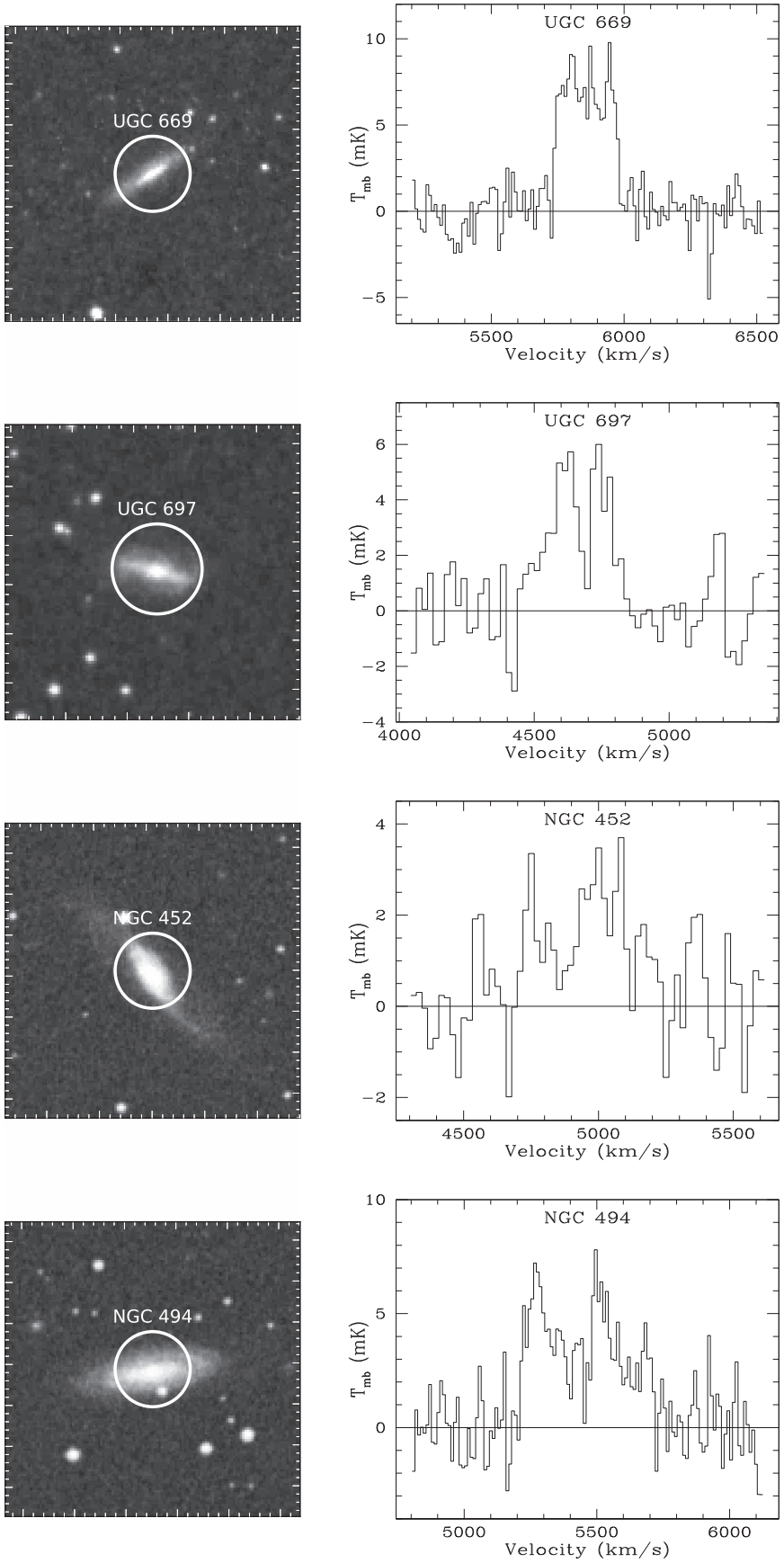

Figure 10. (Continued.)

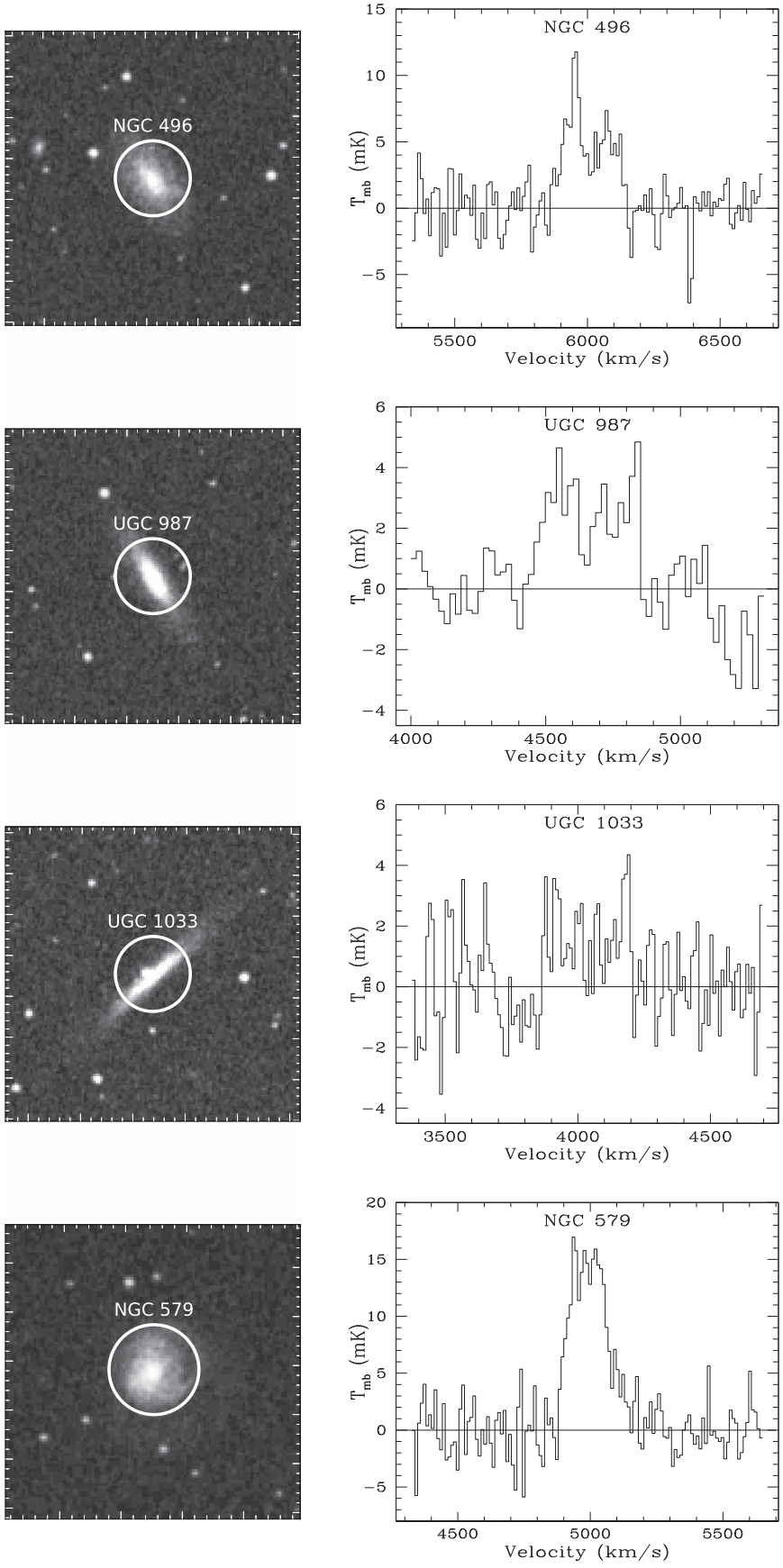

Figure 10. (Continued.)

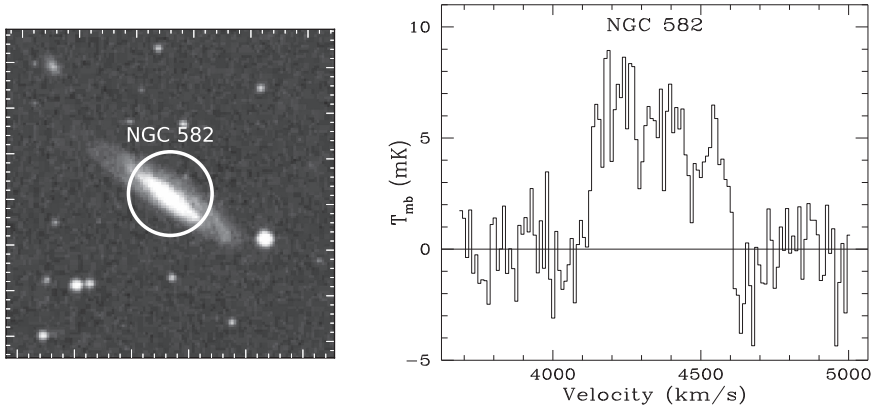

Figure 10. (Continued.)

Table 2
CO Observational Results of Sample Galaxies

Galaxy	T_{mb}^{peak} (mK)	rms (mK)	W_{20p}[a] (km s^{-1})	W_{50p}[a] (km s^{-1})	V_{sys} (km s^{-1})	CO flux[b] (Jy km s^{-1})	M_{H_2}[c] (10^9 $M_\odot$)
UGC 0501	6.8	2.4	460 (9)	365 (64)	5043	49.4 (10.6)	2.1 (0.5)
UGC 0540	4.3	1.8	402 (8)	273 (76)	4983	28.0 (7.8)	1.2 (0.3)
UGC 0556	15.2	2.4	435 (3)	410 (10)	4632	105.1 (7.3)	4.5 (0.3)
PGC 3275	6.3	1.6	220 (9)	183 (5)	5152	21.0 (3.6)	0.9 (0.2)
UGC 0575	3.1	1.5	473 (9)	424 (79)	4692	17.9 (6.7)	0.8 (0.3)
UGC 0623	5.0	2.6	352 (7)	340 (15)	4841	34.8 (11.4)	1.5 (0.5)
UGC 0669	9.8	1.3	246 (1)	231 (5)	5858	45.2 (3.9)	1.9 (0.2)
UGC 0697	6.0	2.4	358 (26)	211 (41)	4665	30.8 (10.3)	1.3 (0.4)
NGC 0452	3.8	1.0	502 (13)	323 (68)	4953	25.5 (4.4)	1.1 (0.2)
NGC 0494	7.7	1.4	500 (2)	474 (13)	5458	50.4 (4.4)	2.2 (0.2)
NGC 0496	11.7	1.8	274 (10)	211 (18)	6014	35.2 (5.7)	1.5 (0.2)
UGC 0987	4.9	2.0	390 (10)	353 (41)	4664	20.5 (9.1)	0.9 (0.4)
UGC 1033	4.3	1.4	334 (2)	327 (6)	4034	14.2 (4.6)	0.6 (0.2)
NGC 0579	16.9	2.2	291 (2)	166 (12)	5009	69.7 (6.8)	3.0 (0.3)
NGC 0582	9.0	1.6	479 (3)	442 (19)	4359	61.2 (5.0)	2.6 (0.2)

Notes. The peak antenna temperature and rms are presented in T_{mb} scale, $T_{mb} = T_R^*/0.88$. Values in parentheses are 1σ uncertainties.
[a] Line widths at 20% and 50% are measured with the second method in the work of Rhee & van Albada (1996). These measured line widths are corrected for instrumental broadening effect, proposed by Verheijen (1997).
[b] Calibration constant CC = 30 Jy K^{-1} is applied to convert the main-beam brightness temperature to Jansky (LD98).
[c] The distance of 60.3 Mpc to the Pisces filament is used to calculate molecular gas mass (Tully & Pierce 2000).

Table 3
Comparison with LD98

Galaxy	T_{int} (minutes)		rms (mK)[a]		W_{20p} (km s^{-1})[b]		W_{50p} (km s^{-1})[b]		CO flux (Jy km s^{-1})[c]	
	LD98	Our obs.	LD98	Our obs.	LD98	Our obs.	LD98	Our obs.	LD98	Our obs.
UGC 0540	270	732	1.9	0.5	202(13)	375(21)	175(17)	250(21)	17.7(3.9)	27.7(3.4)
UGC 0556	117	225	4.8	1.5	442(12)	437(21)	413(7)	395(21)	87.0(6.9)	103.5(7.3)

Notes. Values in parentheses are 1σ uncertainties.
[a] The rms is presented in T_{mb} scale, $T_{mb} = T_R^*/0.88$.
[b] The line widths at 20% and 50% are measured using the method described in Lavezzi & Dickey (1997). No correction is applied to the estimated line widths.
[c] The calibration constant CC = 30 Jy K^{-1} is applied to convert the main-beam brightness temperature to Jansky (LD98).

A.3. Extrapolation of the Central Beam

Because of the large distance to the Pisces cluster, the optical angular size is comparable with the telescope beam size, and a single beam observation has been done only at the central position. There are several extrapolation methods to use a single beam CO observation (e.g., Saintonge et al. 2011a; Lisenfeld et al. 2011; Boselli et al. 2014a, 2014b, 2014c), and we examined three extrapolation methods from the central beam flux to the total flux to lower the uncertainty of the CO data due to any possible missing flux.

The first one is from Saintonge et al. (2011a), who used full mapping CO data for 40 nearby galaxies (Kuno et al. 2007) and derived a simple empirical relationship between the central

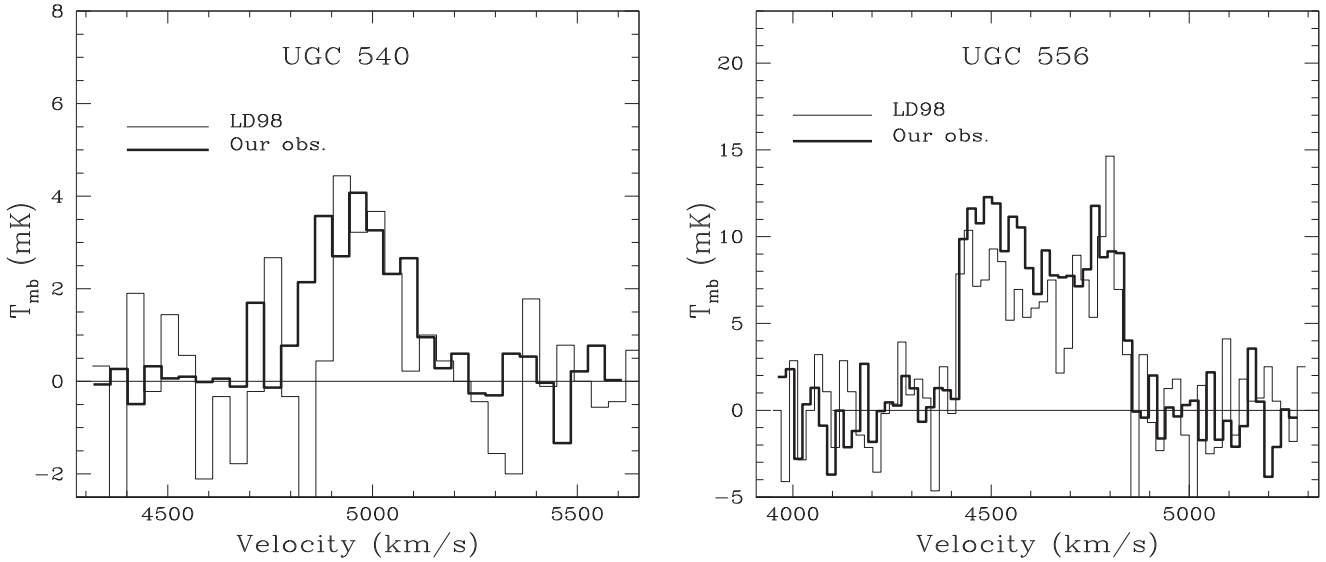

Figure 11. CO spectra of UGC 540 and UGC 556. The solid lines represent the spectra of LD98 and the thick solid lines represent the spectra of our observations. The spectra of UGC 540 and UGC 556 are reproduced in this work. The axes are the main-beam brightness temperature T_{mb} in mK and heliocentric velocity in km s^{-1}. The CO spectrum of UGC 540 is binned to 42 km s^{-1} velocity resolution, and that of UGC 556 is three-channel box smoothed and then binned to 21 km s^{-1} velocity resolution.

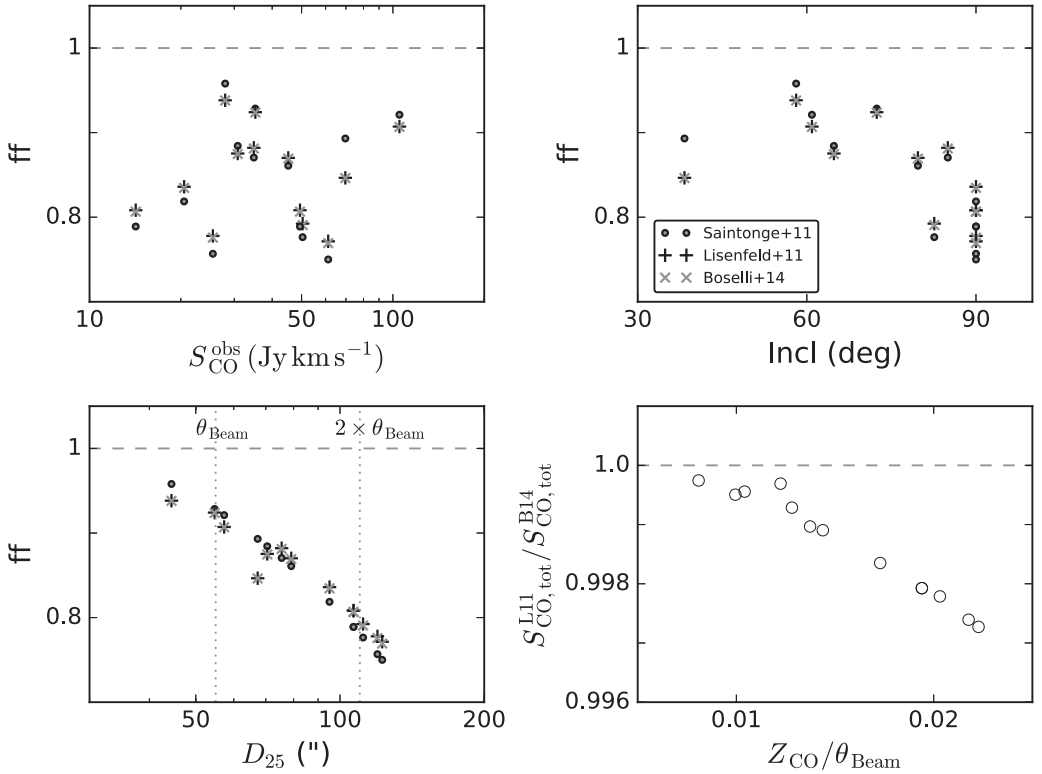

Figure 12. Relationships between the filling factor, ff, defined as the fraction of CO flux covered by the central beam to the extrapolated total CO flux following the method of Saintonge et al. (2011a, dot), Lisenfeld et al. (2011, plus), and Boselli et al. (2014a, gray cross), and the central beam flux (S_{CO}^{obs}, top left), inclination (top right), and optical diameter (bottom left) are presented. The bottom-right panel shows the ratio of the corrected total CO flux obtained by the two-dimensional and three-dimensional prescriptions of Lisenfeld et al. (2011) and Boselli et al. (2014a, 2014b, 2014c) as a function of the molecular gas scale height ratio to the beam size (Z_{CO}/θ_{beam}).

beam flux and the optical size and total flux of a galaxy: $S_{CO,cor} = S_{CO,obs}/(1.094 - 0.008 \times D_{25} + 2.0 \times 10^{-5} \times D_{25}^2)$, where $S_{CO,cor}$ is the extrapolated total flux, $S_{CO,obs}$ the observed flux, and D_{25} the optical diameter.

Second, we applied the method of Lisenfeld et al. (2011), in which the exponential CO distribution with a CO scale length, r_e/r_{25}, of ~0.2 is assumed, i.e., $I_{CO}(r) = I_0 \exp(-r/r_e)$, where I_0 is the central CO flux, and calculated the aperture-corrected total CO flux.

The last one we adopted is from Boselli et al. (2014a, 2014b, 2014c), who modified the two-dimensional prescription of Lisenfeld et al. (2011). They considered the thickness of the CO by assuming the scale height of the molecular gas disk, z_{CO}, as ~0.01 r_{25} at the *B*-band and derived the total CO

flux: $S_{\rm CO,tot} = \int_{-\infty}^{\infty}\int_{0}^{\infty}\int_{0}^{2\pi} rS_{\rm CO}(r, z)\, d\theta dr dz$. This modified method shows the same extrapolated result as in Lisenfeld et al. (2011), except for highly inclined galaxies ($i > 80°$) (Boselli et al. 2014a, 2014b, 2014c).

The results are shown in Figure 12. The filling factor is 75%–95% for all three methods. The methods of Lisenfeld et al. (2011) and Boselli et al. (2014a, 2014b, 2014c) agree well with each other, but the method of Saintonge et al. (2011a) gives a slightly smaller or larger total CO flux than the results of the other two methods. The relationships with the inclination and optical diameter (the top-right and bottom-left panels in Figure 12) show that the result of the Saintonge et al. (2011a) method is smaller for inclined and large-size galaxies and larger for galaxies with a low inclination and small optical size than the other two prescriptions. However, the difference is not significant ($|S^{\rm S11}_{\rm CO,tot} - S^{\rm B14}_{\rm CO,tot}|/S^{\rm L11}_{\rm CO,tot} < 0.05$, where $S^{\rm S11}_{\rm CO,tot}$ and $S^{\rm B14}_{\rm CO,tot}$ is the total CO flux extrapolated following Saintonge et al. 2011a and Boselli et al. 2014a, 2014b, 2014c, respectively). The bottom-right panel in Figure 12 shows the relationship between the ratios obtained by Lisenfeld et al. (2011) and Boselli et al. (2014a, 2014b, 2014c; $S^{L11}_{\rm CO,tot}/S^{B14}_{\rm CO,tot}$) and the ratio of the molecular gas scale height of the disk to the telescope beam size ($Z_{\rm CO}/\theta_{\rm Beam}$), and the decreasing trend with increasing $Z_{\rm CO}/\theta_{\rm Beam}$ is similar to that shown in Boselli et al. (2014a, 2014b, 2014c). However, the difference is not large, less than 0.3%, and this is because our Pisces galaxies have a small $Z_{\rm CO}/\theta_{\rm Beam}$, i.e., $D_{25}/\theta_{\rm Beam} \lesssim 2$. We chose the method used by Boselli et al. (2014a, 2014b, 2014c) and used the corrected total CO flux for our analyses.

References

Arp, H. 1968, PASP, 80, 129
Balogh, M. L., Schade, D., Morris, S. L., et al. 1998, ApJL, 504, L75
Bekki, K., Couch, W. J., & Shioya, Y. 2002, ApJ, 577, 651
Bigiel, F., & Blitz, L. 2012, ApJ, 756, 183
Binney, J., Dehnen, W., & Bertelli, G. 2000, MNRAS, 318, 658
Böhringer, H., Briel, U. G., Schwarz, R. A., et al. 1994, Natur, 368, 828
Boissier, S., Boselli, A., Duc, P. A., et al. 2012, A&A, 545, 142
Bolatto, A. D., Wolfire, M., & Leroy, A. K. 2013, ARA&A, 51, 207
Boselli, A., Boissier, S., Heinis, S., et al. 2011, A&A, 528, 107
Boselli, A., Cortese, L., & Boquien, M. 2014a, A&A, 564, 65
Boselli, A., Cortese, L., Boquien, M., et al. 2014b, A&A, 564, 66
Boselli, A., Cortese, L., Boquien, M., et al. 2014c, A&A, 564, 67
Boselli, A., Cuillandre, J. C., Fossati, M., et al. 2016a, A&A, 587, 68
Boselli, A., Lequeux, J., & Gavazzi, G. 2002, A&A, 384, 33
Boselli, A., Roehlly, Y., Fossati, M., et al. 2016b, A&A, 596, 11
Boselli, A., Tuffs, R. J., Gavazzi, G., Hippelein, H., & Pierini, D. 1997, A&AS, 121, 507
Bosma, A. 1991, in Warped Disks and Inclined Rings around Galaxies, ed. S. Casertano, P. D. Sackett, & F. H. Briggs (Cambridge: Cambridge Univ. Press), 181
Bravo-Alfaro, H., Cayatte, V., van Gorkom, J. H., & Balkowski, C. 2000, AJ, 119, 580
Brosch, N., Formiggini, L., Almoznino, E., et al. 1997, ApJS, 111, 143
Cao, C., Xu, C. K., Domingue, D., et al. 2016, ApJS, 222, 16
Casoli, F., Boisse, P., Combes, F., & Dupraz, C. 1991, A&A, 249, 359
Cayatte, V., Kotanyi, C., Balkowski, C., & van Gorkom, J. H. 1994, AJ, 107, 1003
Cayatte, V., van Gorkom, J. H., Balkowski, C., & Kotanyi, C. 1990, AJ, 100, 604
Chamaraux, P., Balkowski, C., & Gerard, E. 1980, A&A, 83, 38
Chen, C.-W., Côté, P., West, A. A., Peng, E. W., & Ferrarese, L. 2010, ApJS, 191, 1
Chung, A., van Gorkom, J. H., Kenney, J. D. P., Crowl, H., & Vollmer, B. 2009a, AJ, 138, 1741
Chung, A., van Gorkom, J. H., Kenney, J. D. P., & Vollmer, B. 2007, ApJL, 659, L115
Chung, E. J., Rhee, M.-H., Kim, H., et al. 2009b, ApJS, 184, 199
Condon, J. J., Cotton, W. D., Greisen, E. W., et al. 1998, AJ, 115, 1693
Cortese, L., Davies, J. I., Pohlen, M., et al. 2010, A&A, 518, 49
Côté, P., Blakeslee, J. P., Ferrarese, L., et al. 2004, ApJS, 153, 223
Crighton, N. H. M., Murphy, M. T., Prochaska, J. X., et al. 2015, MNRAS, 452, 217
Crowl, H. H., & Kenney, J. D. P. 2008, AJ, 136, 1623
Cybulski, R., Yun, M. S., Fazio, G. G., & Gutermuth, R. A. 2014, MNRAS, 439, 3564
Dekel, A., & Birnboim, Y. 2006, MNRAS, 368, 2
Devereux, N. A., & Young, J. S. 1990, ApJ, 350, 25
Dressler, A. 1980, ApJ, 236, 351
Fraternali, F., & Tomassetti, M. 2012, MNRAS, 426, 2166
Fu, J., Guo, Q., Kauffmann, G., & Krumholz, M. R. 2010, MNRAS, 409, 515
Fumagalli, M., Cantalupo, S., Dekel, A., et al. 2016, MNRAS, 462, 1978
Fumagalli, M., Krumholz, M. R., Prochaska, J. X., Gavazzi, G., & Boselli, A. 2009, ApJ, 697, 1811
Gavazzi, G., Boselli, A., Pedotti, P., Gallazzi, A., & Carrasco, L. 2002a, A&A, 386, 114
Gavazzi, G., Boselli, A., Pedotti, P., Gallazzi, A., & Carrasco, L. 2002b, A&A, 396, 449
Gavazzi, G., Pierini, D., & Boselli, A. 1996, A&A, 312, 397
Genzel, R., Tacconi, L. J., Lutz, D., et al. 2015, ApJ, 800, 20
Geréb, K., Catinella, B., Cortese, L., et al. 2016, MNRAS, 462, 382
Giovanelli, R., & Haynes, M. P. 1983, AJ, 88, 881
Giovanelli, R., & Haynes, M. P. 1985, AJ, 90, 2445
Giovanelli, R., Haynes, M. P., Kent, B. R., et al. 2007, AJ, 133, 2569
Gunn, J. E., & Gott, J. R. I. 1972, ApJ, 176, 1
Hanski, M. O., Theureau, G., Ekholm, T., & Teerikorpi, P. 2001, A&A, 378, 345
Hardcastle, M. J., Worrall, D. M., Birkinshaw, M., Laing, R. A., & Bridle, A. H. 2002, MNRAS, 334, 182
Haynes, M. P., & Giovanelli, R. 1984, AJ, 89, 758
Haynes, M. P., & Giovanelli, R. 1986, ApJL, 306, L55
Helou, G., Khan, I. R., Malek, L., & Boehmer, L. 1988, ApJS, 68, 151
Hewitt, J. N., Haynes, M. P., & Giovanelli, R. 1983, AJ, 88, 272
Hibbard, J. E., van Gorkom, J. H., Rupen, M. P., & Schiminovich, D. 2001, in ASP Conf. Ser. 240, Gas and Galaxy Evolution, ed. J. E. Hibbard, J. H. van Gorkom, & M. P. Rupen (San Francisco, CA: ASP), 657
Hopkins, A. M., & Beacom, J. F. 2006, ApJ, 651, 142
Jaffé, Y. L., Verheijen, M. A. W., Haines, C. P., et al. 2016, MNRAS, 461, 1202
Jarrett, T. H., Chester, T., Cutri, R., Schneider, S. E., & Huchra, J. P. 2003, AJ, 125, 525
Kauffmann, G., Li, C., Fu, J., et al. 2012, MNRAS, 422, 997
Kenney, J. D., Wong, I., Kenney, Z., et al. 2012, in American Astronomical Society Meeting Abstracts 219, 246.03
Kenney, J. D., & Young, J. S. 1988, ApJS, 66, 261
Kenney, J. D. P., Geha, M., Jáchym, P., et al. 2014, ApJ, 780, 119
Kenney, J. D. P., & Young, J. S. 1989, ApJ, 344, 171
Kennicutt, R. C. J. 1983, AJ, 88, 483
Kennicutt, R. C. J. 1998, ApJ, 498, 541
Kim, D.-W., & Fabbiano, G. 1995, ApJ, 441, 182
Kim, S., Rey, S.-C., Jerjen, H., et al. 2014, ApJS, 215, 22
Kodama, T., Smail, I., Nakata, F., Okamura, S., & Bower, R. G. 2001, ApJL, 562, L9
Komossa, S., & Böhringer, H. 1999, A&A, 344, 755
Koopmann, R. A., & Kenney, J. D. P. 2004a, ApJ, 613, 851
Koopmann, R. A., & Kenney, J. D. P. 2004b, ApJ, 613, 866
Koopmann, R. A., Kenney, J. D. P., & Young, J. 2001, ApJS, 135, 125
Kraft, R. P., Forman, W. R., Churazov, E., et al. 2004, ApJ, 601, 221
Krumholz, M. R., McKee, C. F., & Tumlinson, J. 2009a, ApJ, 693, 216
Krumholz, M. R., McKee, C. F., & Tumlinson, J. 2009b, ApJ, 699, 850
Kuno, N., & Nakai, N. 1997, PASJ, 49, 279
Kuno, N., Sato, N., Nakanishi, H., et al. 2007, PASJ, 59, 117
Larson, R. B. 2003, RPPh, 66, 1651
Lavezzi, T. E., & Dickey, J. M. 1997, AJ, 114, 2437
Lavezzi, T. E., & Dickey, J. M. 1998, AJ, 115, 405
Lee, B., Chung, A., Tonnesen, S., et al. 2017, MNRAS, 466, 1382
Lee, M.-Y. 2007, Master's thesis, Yonsei Univ.
Leroy, A. K., Walter, F., Bigiel, F., et al. 2009, AJ, 137, 4670
Leroy, A. K., Walter, F., Brinks, E., et al. 2008, AJ, 136, 2782
Lisenfeld, U., Espada, D., Verdes-Montenegro, L., et al. 2011, A&A, 534, 102
Lisker, T., Glatt, K., Westera, P., & Grebel, E. K. 2006a, AJ, 132, 2432
Lisker, T., Grebel, E. K., & Binggeli, B. 2006b, AJ, 132, 497
Lisker, T., Grebel, E. K., & Binggeli, B. 2008, AJ, 135, 380

Lisker, T., Grebel, E. K., Binggeli, B., & Glatt, K. 2007, ApJ, 660, 1186
Mei, S., Blakeslee, J. P., Côté, P., et al. 2007, ApJ, 655, 144
Mok, A., Wilson, C. D., Golding, J., et al. 2016, MNRAS, 456, 4384
Murphy, E. J., Condon, J. J., Schinnerer, E., et al. 2011, ApJ, 737, 67
Nakai, N., Kuno, N., Handa, T., & Sofue, Y. 1994, PASJ, 46, 527
Nehlig, F., Vollmer, B., & Braine, J. 2016, A&A, 587, 108
Neugebauer, G., Habing, H. J., van Duinen, R., et al. 1984, ApJ, 278, 1
Noordermeer, E., & Verheijen, M. A. W. 2007, MNRAS, 381, 1463
Odekon, M. C., Koopmann, R. A., Haynes, M. P., et al. 2017, ApJ, 824, 110
Pak, M., Rey, S.-C., Lisker, T., et al. 2014, MNRAS, 445, 630
Penny, S. J., Masters, K. L., Weijmans, A.-M., et al. 2016, MNRAS, 462, 3955
Perea, J., del Olmo, A., Verdes-Montenegro, L., & Yun, M. S. 1997, ApJ, 490, 166
Putman, M. E., Peek, J. E. G., & Joung, M. R. 2012, ARA&A, 50, 491
Rengarajan, T. N., & Iyengar, K. V. K. 1992, MNRAS, 259, 559
Rhee, M. H., Chung, A., Verheijen, M., & Yun, M. S. 2001, in IAU Symp. 205, Galaxies and their Constituents at the Highest Angular Resolutions, ed. R. T. Schilizzi (San Francsico, CA: ASP), 350
Rhee, M. H., & van Albada, T. S. 1996, A&AS, 115, 407
Roberts, M. S., & Haynes, M. P. 1994, ARA&A, 32, 115
Saintonge, A., Kauffmann, G., Kramer, C., et al. 2011a, MNRAS, 415, 32
Saintonge, A., Kauffmann, G., Wang, J., et al. 2011b, MNRAS, 415, 61
Sakai, S. 1995, PhD thesis, Waseda Univ.
Sakai, S., Giovanelli, R., & Wegner, G. 1994, AJ, 108, 33
Sánchez Almeida, J., Elmegreen, B. G., Muñoz-Tuñón, C., & Elmegreen, D. M. 2014, A&ARv, 22, 71
Sancisi, R., Fraternali, F., Oosterloo, T., & van der Hulst, T. 2008, A&ARv, 15, 189
Sanders, D. B., Mazzarella, J. M., Kim, D. C., Surace, J. A., & Soifer, B. T. 2003, AJ, 126, 1607
Scott, T. C., Usero, A., Brinks, E., et al. 2013, MNRAS, 429, 221
Scoville, N., Lee, N., Vanden Bout, P., et al. 2017, ApJ, 837, 150
Scoville, N., Sheth, K., Aussel, H., et al. 2016, ApJ, 820, 83
Serra, P., Oosterloo, T., Morganti, R., et al. 2012, MNRAS, 422, 1835
Sorai, K., Nakai, N., Kuno, N., Nishiyama, K., & Hasegawa, T. 2000, PASJ, 52, 785
Stark, A. A., Knapp, G. R., Bally, J., et al. 1986, ApJ, 310, 660
Tully, R. B., & Pierce, M. J. 2000, ApJ, 533, 744
Tully, R. B., Verheijen, M. A. W., Pierce, M. J., Huang, J.-S., & Wainscoat, R. J. 1996, AJ, 112, 2471
van der Hulst, J. M., Terlouw, J. P., Begeman, K. G., Zwitser, W., & Roelfsema, P. R. 1992, in ASP Conf. Ser. 25, Astronomical Data Analysis Software and Systems I, ed. D. M. Worrall, C. Biemesderfer, & J. Barnes (San Francisco, CA: ASP), 131
van Gorkom, J. H., Balkowski, C., & Kotanyi, C. 1984, Clusters and Groups of Galaxies (Springer Netherlands: Dordrecht)
Verdes-Montenegro, L., Yun, M. S., Perea, J., del Olmo, A., & Ho, P. T. P. 1998, ApJ, 497, 89
Verheijen, M. A. W. 1995, ApL&C, 31, 349
Verheijen, M. A. W. 1997, PhD thesis, Univ. Groningen
Verheijen, M. A. W. 2001, in ASP Conf. Ser. 240, Gas and Galaxy Evolution, ed. J. E. Hibbard, J. H. van Gorkom, & M. P. Rupen (San Francisco, CA: ASP), 573
Verheijen, M. A. W. 2004, in IAU Coll. 195, Outskirts of Galaxy Clusters: Intense Life in the Suburbs, ed. A. Diaferio (Cambridge: Cambridge Univ. Press), 394
Verheijen, M. A. W., & Sancisi, R. 2001, A&A, 370, 765
Vollmer, B., Balkowski, C., Cayatte, V., van Driel, W., & Huchtmeier, W. 2004, A&A, 419, 35
Vollmer, B., Cayatte, V., Balkowski, C., & Duschl, W. J. 2001, ApJ, 561, 708
Voyer, E. N., Boselli, A., Boissier, S., et al. 2014, A&A, 569, 124
Walter, F., Brinks, E., de Blok, W. J. G., et al. 2008, AJ, 136, 2563
Warmels, R. H. 1986, HI Properties of Spiral Galaxies in the Virgo Cluster (Groningen: Rijksuniversiteit)
Warmels, R. H. 1988, A&AS, 72, 427
Watkins, A. E., Mihos, J. C., Harding, P., & Feldmeier, J. J. 2014, ApJ, 791, 38
Whitmore, B. C., Gilmore, D. M., & Jones, C. 1993, ApJ, 407, 489
Wolfinger, K., Kilborn, V. A., Koribalski, B. S., et al. 2013, MNRAS, 428, 1790
Wolfinger, K., Kilborn, V. A., Ryan-Weber, E. V., & Koribalski, B. S. 2016, PASA, 33, 38
Young, J. S., Allen, L., Kenney, J. D. P., Lesser, A., & Rownd, B. 1996, AJ, 112, 1903
Young, J. S., & Scoville, N. Z. 1991, ARA&A, 29, 581
Young, J. S., Xie, S., Tacconi, L., et al. 1995, ApJS, 98, 219
Zabludoff, A. I., & Mulchaey, J. S. 1998, ApJ, 496, 39